

Review of studies on fundamental issues in LBE corrosion¹

Jinsuo Zhang^{a2}, Ning Li^b

^a Decision Application Division,
Center for Nonlinear Studies,
Los Alamos National Laboratory
Los Alamos, New Mexico, USA

^b Material Science and Technology Division,
Los Alamos National Laboratory
Los Alamos, New Mexico, USA

Abstract. Lead bismuth eutectic (LBE) technology is being developed for applications in advanced nuclear systems and high power spallation neutron target. In this paper, the current understanding of corrosion and the fundamental issues relevant to corrosion when using LBE as a heavy liquid metal nuclear coolant are reviewed. Corrosion mechanisms and processes in LBE are examined. Prospective methods to mitigate corrosion are briefly reviewed. We then discuss the oxygen control technique for corrosion mitigation in detail, including the range of oxygen concentrations in LBE, oxygen sensors, and the surface oxidation kinetics. Existing experimental results are summarized and reviewed. Theoretical corrosion models for non-isothermal liquid metal loops are refined and compared each other. The applications of these models to a few practical lead alloy systems are used to illustrate the corrosion mechanisms and the parameter dependency, and to benchmark. Based on the current state of knowledge, a number of R&D tasks are proposed to fill the gaps and firmly establish the scientific underpinning before LBE nuclear coolant technology is ready for programmatic and industrial applications.

1. Introduction

Lead bismuth eutectic (LBE) has been a primary candidate material for high-power spallation neutron targets and coolant in accelerator-driven systems (ADS) and coolant in advanced nuclear reactors due to its favorable thermal-physical and chemical properties. These include the low melting point, low vapor pressure, wide margin to boiling, high spallation neutron yield, low neutron moderation and capture, and chemical inertness resulting in mild reaction with air and water. However, it is well known that steels are severely corroded by LBE if they are exposed to LBE directly at medium to high temperatures. Corrosion of containment and structural materials presents a critical challenge in the use of LBE in ADS and advanced nuclear reactors. Full knowledge of the important characteristics of the flow-induced and/or enhanced corrosion is essential in the proper design and safe operation of LBE heat transfer circuits. Currently a lack of systematic understanding of the scientific basis is limiting many R&D efforts to testing and impeding the development of material and technologies. Several efforts are underway to remedy this deficiency, including the preparation of an LBE materials handbook by an international expert group.

The present paper reviews the current understanding of steel corrosion in LBE and the associated fundamental issues when using LBE as a nuclear coolant. The relevant physical and chemical properties are included. The dissolution of materials into LBE and the diffusion coefficients for corrosion products in LBE is presented. The following important aspects of

¹ LA-UR-04-0869. This research supported by Department of Energy under contact number W-7405-ENG-36

² Present address: Center for Nonlinear Studies, MS-B258; Los Alamos National Laboratory, Los Alamos, NM 87545, USA; Tel: (505) 667-7444; Fax: (505) 665-2659; E-mail: jzhang@cnls.lanl.gov.

LBE corrosion are reviewed: corrosion mechanisms, environmental effects, oxygen control technology for steel corrosion mitigation, existing experimental data, and the corrosion modeling results. We also outline the needed future studies to fill the gaps and establish the scientific underpinning before LBE nuclear coolant is ready for programmatic and industrial applications.

The rest of the paper is organized as the following:

- Section 2 presents the materials information on LBE, including phase diagram, activity of each component and physical properties.
- Section 3 analyzes the corrosion phenomena in LBE, including corrosion mechanisms, corrosion product solubility, diffusion and transport in LBE, factors affecting the corrosion processes and methods for mitigating corrosion.
- Section 4 summarizes the active oxygen control technique for protection of structure steels, including oxygen activity, solubility and diffusion coefficient in LBE, controlling processes and oxygen sensors.
- Sections 5 and 6 present recent experimental and theoretical (corrosion modeling).
- Section 7 outlines our recommendations of important subjects for near future studies.

2. Lead-Bismuth Eutectic Alloy

The first step in evaluation of an alloy system is to establish the phase diagram. The lead bismuth alloy phase diagram was given by Hansen and Anderko [1], Elliott [2], and Hultgren *et al.* [3]. The most recent update of the phase diagram was by the Institute of Physics and Power Engineering (IPPE) in Obninsk, Russia, for the purpose of using lead-bismuth alloy as a nuclear coolant [4].

2.1. Phase Diagram of Lead-Bismuth Alloy

The phase diagram by IPPE is shown in Fig. 1. It indicates that the eutectic point is 123.5°C at 44.8 wt% of lead. The melting points of pure lead and pure bismuth are 327°C and 271°C, respectively. There is a small difference between the eutectic points reported by IPPE and Elliot [2], who reported the eutectic point of 125.5°C at 44.5 wt% of lead. For our discussions, the alloy with 44.8 wt% Pb and 55.2 wt% Bi (corresponding to 45.0 at% Pb and 55.0 at% Bi) is considered the lead-bismuth eutectic (LBE) [4].

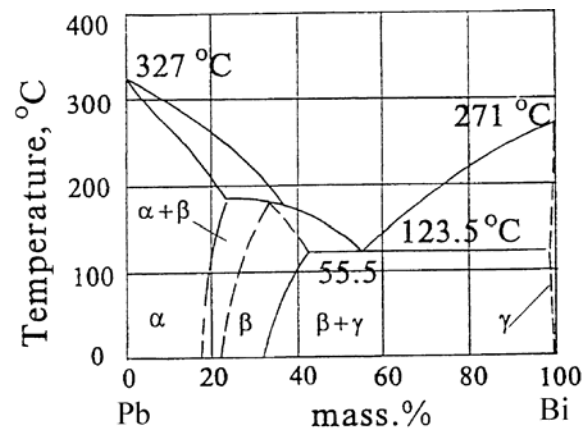


FIG. 1. Pb-Bi phase diagram obtained by the Institute of Physics and Power Engineering, Obninsk, Russia. α is Pb, β is Pb₇Bi₃ and γ is Bi.

2.2. Thermodynamic Properties of Lead-Bismuth Alloy

The determination of thermodynamic and structural properties of liquid lead-bismuth alloy has been the subject of numerous investigations using various techniques such as vapor-pressure measurement [5-6], electromotive force (EMF) measurements [7-11], mass spectrometry [12], and electrochemical measurement using solid electrolyte [13]. A critical analysis of the earlier studies (before 1973) was presented by Hultgren et al. [3].

For calculating the activity coefficients of the binary solutions, Krupkowski's formulae take the form [10]:

$$\ln \gamma_1 = \omega(T)(1 - X_1)^m, \quad (1a)$$

$$\ln \gamma_2 = \omega(T) \left[X_2^m - \frac{m}{m-1} X_2^{m-1} + \frac{1}{m-1} \right], \quad (1b)$$

where γ_i and X_i ($i = 1, 2$) are the activity coefficient and the atom fraction of the metal i , the $\omega(T)$ function characterizes the degrees of regularity of the system, the exponent m is the asymmetry coefficient and the T is the temperature in Kelvin. It was found that Eq. 1a applies mostly to the component having the smaller atomic radius in the systems [10]. The activity of the metal i in the alloy is:

$$a_i = \gamma_i X_i \quad (2)$$

For liquid lead bismuth alloys, it was reported that the exponent m equals 2 [10]. The function $\omega(T)$, independent of the alloy composition, is different for different temperature ranges. Moser [10] reported that in the range of 670-760 K, $\omega(T) = -[447/T + 0.2025]$, while in the range of 1150-1320 K, Prasad et al. [6] reported that $\omega(T) = -[391.5/T + 0.2693]$. Therefore, the activity coefficient of Pb and Bi in the liquid alloy can be written as:

$$\ln \gamma_{Pb} = \omega(T)(1 - X_{Pb})^2, \quad (3a)$$

$$\ln \gamma_{Bi} = \omega(T)(1 - X_{Bi})^2, \quad (3b)$$

in the range of 670-760 K :

$$\omega(T) = -[447/T + 0.2025],$$

and the in range of 1150-1320 K:

$$\omega(T) = -[391.5/T + 0.2693].$$

These correlations were verified by experiments. For the range of 760-1150 K, we did not find validated correlations of $\omega(T)$. Mikula [11] carried out detailed studies in the 643-923 K temperature range using the EMF method. A global $\omega(T)$ was given by IPPE [7] for LBE as:

$$\omega(T) = -[446.97/T + 0.2026].$$

2.3. Physical Properties of Lead-Bismuth Eutectic

Lead and lead-bismuth eutectic emerged as leading candidates for nuclear coolant and high-power spallation targets [14,15] because of their high atomic numbers, low melting points, and high boiling points (1725°C for pure lead, 1670°C for LBE) [16]. LBE has exceptional chemical, thermal physical, nuclear, and neutronic properties well suited for nuclear coolant spallation target applications [17]. In particular, lead-bismuth alloys do not react violently

with air (oxygen) and water, which enhances the safety of lead-alloys-cooled reactors [16]. The liquid binary alloy of lead and bismuth (LBE) is also thermodynamically near the ideal solution [18]. Density and viscosity are important physical properties of LBE as a nuclear coolant and relevant to corrosion influenced by hydrodynamic conditions. Both are functions of temperature. Generally, density ρ and dynamic viscosity μ can be written as:

$$\rho(T) = (A_\rho - B_\rho T) \times 10^3, \quad (4)$$

$$\mu(T) = A_\mu \times 10^{-3} \exp(E / RT), \quad (5)$$

where A , B , and E are constant, $R = 8.314 \text{ JK}^{-1} \text{ mol}^{-1}$ is the gas constant. The literature reported for

- pure lead: $A_\rho = 11.4478 \text{ kgm}^{-3}$ and $B_\rho = 0.00131 \text{ kgK}^{-1} \text{ m}^{-3}$ [19],
- and $A_\mu = 0.5449 \text{ kgm}^{-1} \text{ s}^{-1}$ and $E = 7694 \text{ Jmol}^{-1}$ [20];
- pure bismuth: $A_\rho = 11.7393 \text{ kgm}^{-3}$ and $B_\rho = 0.00127 \text{ kgK}^{-1} \text{ m}^{-3}$ [21],
- $A_\mu = 0.4380 \text{ kgm}^{-1} \text{ s}^{-1}$ and $E = 6432 \text{ Jmol}^{-1}$ [22];
- for LBE $A_\rho = 11.060 \text{ kgm}^{-3}$ and $B_\rho = 0.00122 \text{ kgK}^{-1} \text{ m}^{-3}$ [23], and
- $A_\mu = 0.4656 \text{ kgm}^{-1} \text{ s}^{-1}$ and $E = 6428 \text{ Jmol}^{-1}$ [24].

Reference [25] gives detailed review of data on pure lead and bismuth. Other data for LBE can be found in Refs. [16,26,27]. The kinematic viscosity ν is calculated from $\nu = \mu / \rho$.

Figure 2 compares the kinematic viscosity of LBE with that of liquid lead and bismuth based on Eqs. 4 and 5. It is shown that pure liquid lead has the largest kinematic viscosity, while pure liquid bismuth has the smallest one at the same temperature. The correlation results for LBE agree very well with the experimental results reported by IPPE [26]. All kinematic viscosities decrease with increasing temperature. Since a smaller kinematic viscosity results in a higher Reynolds number, decreasing kinematic viscosity with temperature results in higher corrosion rates in mass diffusion limited situations.

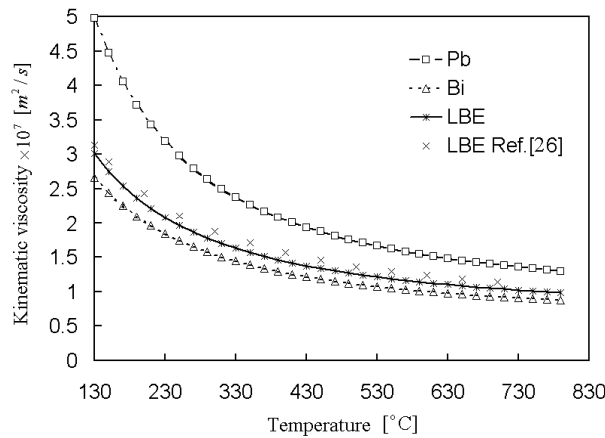


FIG. 2. Comparisons of the kinematic viscosities of liquid lead, bismuth, and LBE.

Another set of important properties of lead-bismuth alloys are the diffusion coefficients of lead and bismuth in their alloys. The diffusion coefficient of each component is important for

understanding the transport kinetics and also for design of equipments for diffusion-limited operating conditions. Mutual diffusion coefficients were measured by Tanigaki et al. [28] for different fractions of Bi in the alloy. Other measured diffusion coefficients of Bi and Pb in their liquid alloys can be found in Refs. [29-31].

3. Corrosion by Lead-Bismuth Eutectic

Corrosion of steels in pure liquid Bi, Pb or LBE occurs primarily through dissolution of steel components into the liquid metals/alloys. The main driving force for liquid metal corrosion is the chemical potential for dissolution of all solid surfaces in contact with the liquids [32]. The compositional and microstructural changes due to selective dissolution and intergranular corrosion can lead to material failures [33]. The dissolution rate depends on the liquid media, the ratio of the surface area of the solid metal to the volume of the liquid metal, the conditions of the surface, the content of interstitial impurities such as oxygen and nitrogen in the liquid metal/alloy and the compositions of the solid materials [34].

3.1. Mechanisms of Liquid Metal/alloy Corrosion

There are two types of corrosion (Fig. 3), uniform and local [34]. Uniform corrosion is characterized by the uniform damage at the surface of the solid phase by the liquid metal. For the local corrosion, the liquid metal penetrates into the solid metal in the areas where zones with a high density of crystal structure defects reach the surface. The local corrosion front moves along grain boundaries, the specific crystallographic directions, vacancies and pores, the previously formed defects (Fig. 3b-3f). The penetration of the liquid metal into solid metals can redistribute the interstitial impurities between the solid and liquid phases [35]. Detailed descriptions of the local or non-uniform corrosion can be found in Ref. [34].

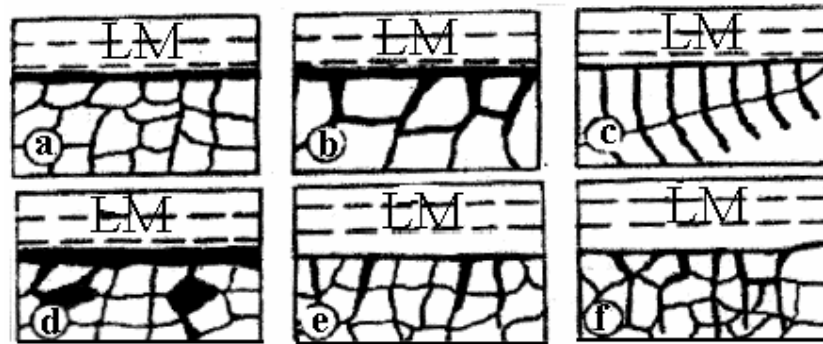


FIG. 3. Diagram of corrosion damage of metals in liquid metal media: (a) uniform corrosion; (b) penetration along the grain boundaries; (c) along the specific crystallographic direction; (d) along vacancies and pores; (e) and (f): along previous formed defects [34]. LM represents the liquid metal.

When liquid metals flow over solid metal/alloy surfaces, the velocity of liquid metals accelerates corrosion. This is called flow accelerated corrosion (FAC) [36]. There are a number of mechanisms for interactions between the flow and dissolution. The combination of different mechanisms results in four main types of flow accelerated corrosion (Fig. 4a-4d): mass transport-controlled corrosion, phase transport-controlled corrosion, erosion-corrosion and cavitation-corrosion [37]. Mass transport-controlled corrosion occurs when the flow velocity is low. The mass transfer rate (combined effects of convection and diffusion) is less than the dissolution rate of the solid metal into the liquid metal, and the corrosion rate is determined by the mass transfer rate. For these cases, the corrosion product concentration at

the solid/liquid interface equals the saturation or equilibrium concentration. For multi-phase flows or high turbulent flows, the aggressive particles in the liquid moving along the protective film surface or the high shear stress at the interface can strip the protective films or wear them away, reducing the thickness of the protective film and leading to erosion-corrosion. In the areas where the flow changes its direction sharply, such as sudden expansions or elbows, the liquid or the aggressive particles are thrown against the surface of solid metals, which results in a higher wear rate. Cavitation-corrosion occurs when there are cavitation bubbles in the flowing liquid metals and the bubbles collapse on solid metal surfaces. The collapse creates micro-jets of the liquid metal to the solid metal surface, producing high local pressure and destroying the surface. This behavior can lead to brief high stress in the solid metal, causing localized corrosion fatigue damage and environmentally assisted micro-fractures of the solid metal.

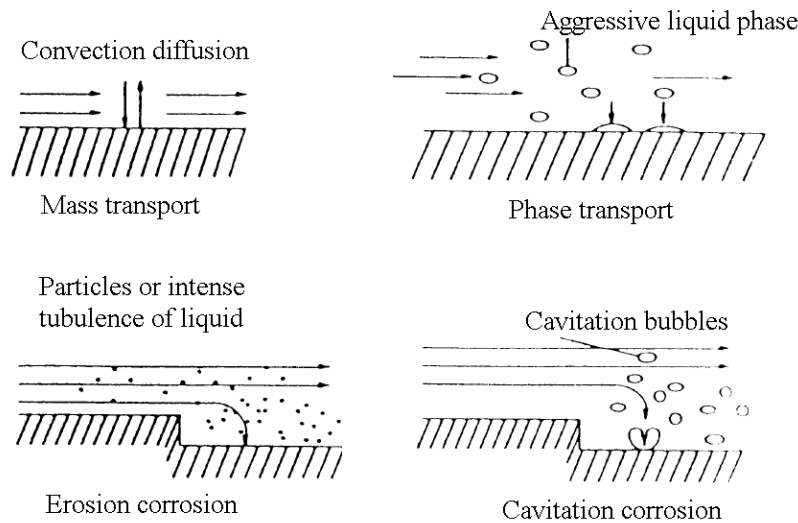


FIG. 4. Representation of the four main types of flow affected corrosion [37].

3.2. Factors Affecting Structural Materials Corrosion in LBE

Liquid metal corrosion process may involve the following four processes [34]:

- (1) dissolution of the solid materials into the liquid metal;
- (2) thermal and concentration gradient assisted mass transfer;
- (3) redistribution of the interstitial impurities between the solid and liquid metals; and
- (4) diffusion penetration of liquid metals into solid metals with formation of solid solutions or new phases.

The operating conditions determine which process dominates. Factors affecting one of the above processes should affect the corrosion rate. These factors are divided into three groups [34]: corrosion, metallurgical, and technological. The corrosion factors include the chemical composition of the liquid metal and its impurity contents, the flowing conditions (the pressure and the flow velocity), the temperature and its profile, the exposure time, etc. The metallurgical factors include the purity of the solid metals, alloying, and the structural state and microstructure of solid materials. The technological factors include the stress state, formation of new phases associated with machining, welding, assembling of structures, and the loading conditions [34].

3.3. Solubility of Metals in Bi, Pb, and LBE

Solubility of iron, chromium, and nickel in lead, bismuth, and LBE plays an important role in corrosion phenomena when using such liquid metals/alloys as nuclear coolants. Experimental measurement of solubilities of potential containment materials has been carried out since the 1950s [16]. Solubilities of various metals in liquid bismuth were summarized by Weeks [38]. However, solubility data of metals in liquid lead and LBE are scarce. IPPE [39] published some correlations of various metal solubilities in LBE. Generally, the saturation solubility of a metal in LBE, lead and bismuth can be written as:

$$\log(c_s, wppm) = A_c + B_c / T(K), \quad (6)$$

where A_c and B_c are constant. Values of the two constants for Fe, Cr, and Ni in liquid LBE, bismuth, and lead are given in Table 1.

TABLE 1. Solubility data of Ni, Fe, and Cr in LBE [39], Bi [38], and Pb [40]

	Fe		Cr		Ni	
	A_c	B_c	A_c	B_c	A_c	B_c
LBE	6.10	-4380	5.08	-2280	7.53	-843
Bi	6.26	-3490	6.86	-3580	6.93	-2400
Pb (673 < T < 873)	4.34	-3450				
Pb (873 < T < 1020)	5.82	-4860				

The solubilities of Fe, Cr, and Ni in LBE are shown in Fig. 5. The solubilities increase quickly with increasing temperature. The solubility of Ni in LBE is much higher than that of Fe and Cr, indicating that Ni content in steels used for containments of LBE needs to be reduced or protected to increase the corrosion resistance.

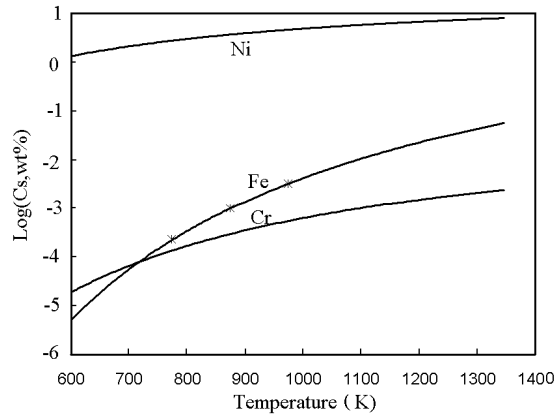


FIG. 5. Variations of solubility of Fe, Cr, and Ni in LBE with temperature. The results are obtained from Eq. 6 for the solid lines. Symbols are solubility data of Fe in LBE obtained experimentally [40].

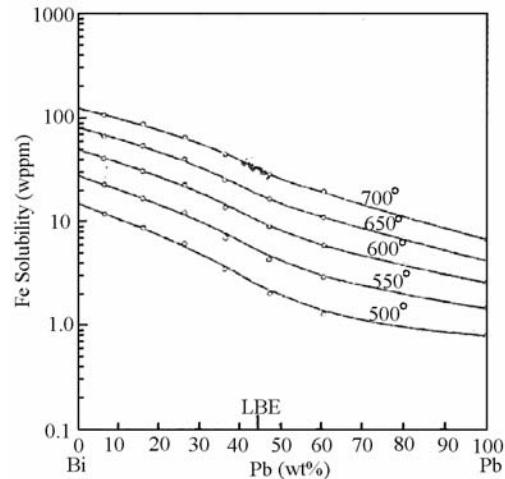


FIG. 6. Variations of the solubility of Fe in lead-bismuth alloy with the alloy composition at different temperatures [40]. The Fe solubility decreases with increasing bismuth fraction, indicating the dissolution corrosion properties of LBE are mainly from bismuth.

The solubility of a metal in liquid lead-bismuth alloys depends on the compositions of the liquid alloy. The dependence of Fe solubility in the liquid lead-bismuth alloy on the lead

content is shown in Fig. 6 [40]. For all the temperatures considered, the Fe solubility decreases with increasing concentration of lead, indicating that the pure liquid lead is less corrosive than LBE. LBE corrosiveness is mainly from the fraction of bismuth in direct dissolution corrosion. As shown in the phase diagram (Fig. 1), the pure lead melting point is higher than that of LBE. A higher operation temperature is needed if liquid lead is used as a nuclear coolant.

3.4. Species Diffusion in LBE

Corrosion products dissolved into LBE at surfaces are transported in LBE for sustained corrosion or stops when the concentrations reach the saturation limits. For static corrosion tests, the transport process is mostly diffusion that depends on the corrosion product concentration gradient and the corrosion product diffusion coefficient in LBE. When the dissolution rate is less than the diffusion rate, diffusion is fast enough to take all the dissolved species and the corrosion rate is determined by the dissolution rate. When the dissolution rate is greater than the diffusion rate, the concentration at the interface is always at saturation and the corrosion rate is determined by the diffusion rate. In liquid metal systems there is good evidence that both cases described above occur [41], depending on the solution and solute.

The diffusion coefficient is a function of temperature. To our best knowledge, there are no experimental correlations for the temperature dependence of diffusion coefficients of Fe, Ni, and Cr in LBE. A single value for iron was reported in the literature [42]:

$$D_{Fe \rightarrow LBE} = 2.27 \pm 0.11 \times 10^{-9} m^2 s^{-1} \text{ at } 750^\circ C.$$

This value is almost same as that of iron in pure lead $D_{Fe \rightarrow Pb} = 2.80 \times 10^{-9} m^2 s^{-1}$ [43] at the same temperature. Therefore, Balbaud-Celerier and Barbier [44] assumed that the diffusion coefficient of iron in LBE equals that in pure lead, and can be calculated using the correlation for lead developed by Robertson [43]:

$$D_{Fe \rightarrow Pb} [m^2/s] = 4.9 \times 10^{-7} \exp\left(-\frac{44100 \pm 6300}{RT}\right). \quad (7)$$

Treating the liquid metal as a continuum, the hydrodynamic theory of diffusion [45] developed a correlation between the diffusion coefficient and the dynamic viscosity by balancing the driving force and the friction force exerted on an atom that has hard sphere shape. The Stokes-Einstein equation is:

$$D [m^2/s] = \frac{kT}{6\pi r \mu}, \quad (8a)$$

where k [J K⁻¹] is the Boltzmann constant and r [m] is the radius of the diffusion atom. The Eyring equation [46] takes the discontinuity in “jump-distance” into account and the diffusion coefficient is written as [47]:

$$D [m^2/s] = \frac{kT}{2r \mu}. \quad (8b)$$

Another correlation is the Sutherland-Einstein equation [44]:

$$D [m^2/s] = \frac{kT}{4\pi r \mu}. \quad (8c)$$

Guminski [48] reported that the diffusion coefficients of dissolved metals in liquid metal/alloy solvents are within one order of magnitude at a given temperature; depending on the solvent metal/alloy large differences cannot be expected based on the Sutherland-Einstein equation.

At 750°C, Eq. 8a-8c predicts the values of Fe diffusion coefficient in LBE are $(6.69, 63.05, 10.04) \times 10^{-9} \text{ m}^2/\text{s}$, respectively. Comparing to the experimental results [43], it seems that the Stokes-Einstein equation (Eq. 8a) is better suited to calculate the species diffusion coefficient in LBE. For pure liquid lead at 750°C, Eq. 7 predicts the Fe diffusion coefficient is in the range of $1.31\text{--}5.75 \times 10^{-9} \text{ m}^2/\text{s}$, while Eq. 8a predicts a value of $4.94 \times 10^{-9} \text{ m}^2/\text{s}$. Therefore, Eq. 8a may be employed to calculate the Fe diffusion coefficient in LBE and lead. In an oxygen control system, the diffusion of oxygen in LBE is particularly important.

3.5. Mass Transfer

In a static isothermal system, transport of corrosion products from surfaces to bulk liquid metals is determined mostly by diffusion. The corrosion process stops when the liquid is saturated with the corrosion products. The situation is quite different in a flowing system. Corrosion products can be transported by both diffusion and convection. The flowing liquid takes corrosion products from dissolution locations to other places where the corrosion products may deposit. Among external factors influencing corrosion, the flow velocity is of the most importance [49]. The effects of the flow velocity for single-phase flow may be summarized as follows [44] (Fig. 7):

- (1) At low velocities, the corrosion is controlled or partially controlled by mass transfer, in other words, the dissolution rate is greater than the mass transfer rate and the corrosion product interface concentration is at saturation. In such cases, the thickness of the laminar mass transfer layer becomes thinner with increasing velocity and as a result the corrosion rate increases.
- (2) When the velocity exceeds a critical value, the mass transfer rate becomes high enough to transport all the corrosion products away for the interface. Then the corrosion rate is determined by the dissolution/reaction rate and independent of the flow velocity. The corrosion is activation controlled.
- (3) For very high velocities, the high shear stress at the interface can strip the protective film on the surface of the structure. Some cavities appear at the interface and corrosion rate increases sharply with the flow velocity. For heavy liquid metals/alloys such as LBE, erosion-corrosion is likely to occur at moderately high velocities due to their high densities.

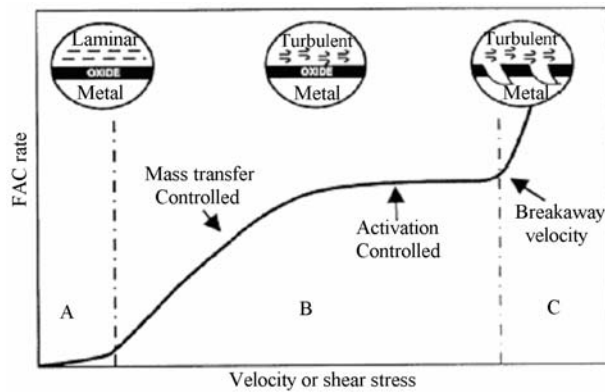


FIG. 7. Velocity effects on the corrosion rate [44].

In practical nuclear coolant system designs, 2 and 3 should be avoided due to rapid and non-uniform corrosion and erosion-corrosion. Therefore, most of the corrosion studies performed for liquid metals/alloys are in the mass transfer controlled regime.

In non-isothermal flowing LBE systems, corrosion products in the hot sections can come out of LBE at some other sections. The corrosion product coming out can exist in the following states [41]:

- (1) The corrosion products deposit on the walls and tightly adhere. A crystal of solute material colliding with the wall and sticking serves as a nucleation center for further deposition. The deposition leads to a small flow area and a higher deposition rate. Once deposition occurs at some location, the feedback is positive and the deposition could block the flow in the long-term run.
- (2) The corrosion product coming out the solution continues to float around in suspension owing to Brownian motions and the fluid flow. The suspension would become more and more concentrated as the process continues, and it is conceivable that it may slow and eventually plug the systems. In this case, the plug may occur in any location including the hot leg where materials are dissolved.
- (3) The solid particles come out of the solution. They are small enough to remain in suspension. When they are carried into the hot zone, due to their small sizes and greater specific surface areas, dissolve at a rate fast compared to that of the wall materials. In this case, the wall would be protected.

The mass transfer of corrosion products in flowing liquid metals/alloys is a complex process. In most of the existing studies on liquid metal corrosion, precipitation/deposition is not adequately considered. Most of the LBE test loops are built for studying materials corrosion. However, sectioning the loops after extended tests may provide valuable information on deposition/precipitation.

3.6. Temperature Effects

The dissolution/chemical reaction rates, the corrosion product diffusion coefficients in solid and liquid alloys and the liquid metal viscosity are functions of temperature. Increasing temperature results in higher dissolution rates, higher solubilities, higher diffusion coefficients, and smaller viscosities. These changes all lead to higher corrosion rates. A sustained corrosion process can only occur in a non-isothermal system such as nuclear coolant systems [50]. In a closed loop system, without temperature gradients, species concentration would eventually reaches a homogeneous distribution and no further corrosion would occur. With temperature gradients, steel elements will be dissolved from the hot legs, transported to locations with lower temperatures, and precipitate. As the temperature gradient increases, attacks in hot sections of loops become more severe [49]. Precipitation in the cold areas can accelerate corrosion in the hot sections [33]. Even for loops have the same highest temperature and other hydraulic parameters, the corrosion rates can different if the loops are operated under different stream-wise temperature profiles [51].

3.7. Approaches for Mitigating Corrosion

The general approaches to reduce the corrosion of structure materials in LBE system are:

- (1) Improving anti-corrosion properties of the structure materials,
- (2) Reducing corrosive effect of the LBE, such as by adding inhibitors or controlling oxygen.

Here we are primarily interested in the second approach. Inhibitors are very effective in reducing the corrosion of steel by forming, for example, carbide and nitride films on the steel surface [52]. Zirconium in Bi [53] and LBE [54] is an effective inhibitor against corrosion of

low-alloy steels. The required concentration of titanium is slightly more difficult to maintain than that of zirconium [52]. The insoluble films formed on the steel surface by the inhibition process change the rate-controlling step from liquid-phase diffusion to diffusion of the dissolving atoms through the film [16]. However these films are brittle and tend to spall, baring fresh surfaces to corrosion. Thus inhibitors must remain in the liquid at all times to insure restoration of the films in spalled areas [53].

If inhibitors are used during the spallation target operations, a variety of spallation products, built up by the interaction of high-energy protons with the target material, will react with the inhibitors in LBE. These reactions may reduce the beneficial effects of the inhibitors [52].

In Russia's heavy liquid metal coolant technology, the oxygen control technique [55] was developed to form protective oxide layers on steel surfaces to reduce the corrosion rate.

The active oxygen control technique exploits the fact that lead and bismuth are chemically less active than the major components of steels, such as *Fe*, *Ni*, and *Cr*. By carefully controlling the oxygen concentration in LBE, it is possible to maintain an iron and chrome based oxide film on the surfaces of structural steels, while keeping lead and bismuth from excessive oxidization that can lead to precipitation contamination. The oxide film effectively separates the substrates from LBE. Once this oxide film is formed on the structure surface, the direct dissolution of the structural materials becomes negligible because the diffusion rates of the alloying components are very small in the oxides [50].

The effects of oxygen in liquid lead on the corrosion behaviors of steels are shown in Fig. 8 [56]. At an oxygen concentration below 10^{-7} at% in lead, corrosion is determined by dissolution of alloy components and the corrosion rate increases significantly with decreasing oxygen concentration. Otherwise, at an oxygen concentration above 10^{-6} at%, oxide films forms on steel surfaces that can prevent the direct dissolution of alloy components. The oxide film thickness depends strongly on the oxygen concentration. To avoid heavy dissolution, oxidation and to remain/restore the protective oxide films, the oxygen concentration in lead alloys needs to be active controlled.

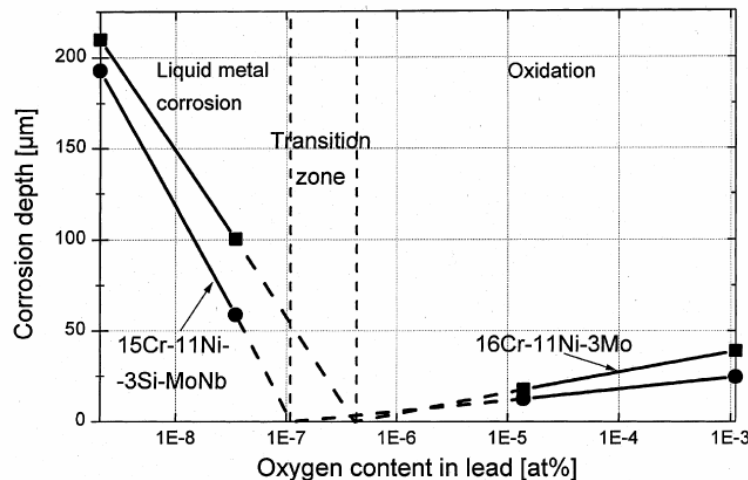


FIG. 8. Oxygen concentration effects on corrosion behavior of steels in flowing pure lead after 3000 hours at 550°C [56].

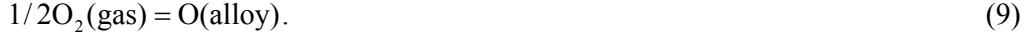
Controlling oxygen in LBE primarily uses gases-in and gas-out processes (although other method are under development), and it is comparatively more feasible and easier to measure

oxygen activity by electrochemical methods. Hence in developing LBE technology, we are primarily interested in this approach.

4. Active Control of Oxygen in Lead-Bismuth Alloy

4.1. Thermodynamics of Oxygen in Lead-Bismuth Alloy

The dissolution of oxygen into liquid lead-bismuth alloy can be expressed as the following chemical reaction:



At equilibrium, the chemical potential of oxygen (gas) is the same as that of oxygen in the alloy. Accordingly, we have [57]:

$$1/2G_{\text{O}_2} = \bar{G}_{\text{O}}, \quad (10)$$

where G_{O_2} is the Gibbs energy of O_2 and \bar{G}_{O} is the partial energy of O in the alloy or the chemical potential of O. If a standard reference is used (pure O_2 at 1 atmosphere), Eq. 10 becomes:

$$P_{\text{O}_2}^{1/2}(\text{gas}) = a_{\text{O}}(\text{alloy}) = \gamma_{\text{O}}X_{\text{O}}, \quad (11)$$

where $P_{\text{O}_2}^{1/2}$ is the partial pressure of O_2 , a_{O} is the activity and X_{O} is the atom fraction of O in the liquid alloy, respectively, γ_{O} is the activity coefficient. According to Wagner [58], the activity coefficient can be expressed in the following Taylor series:

$$\ln \gamma_{\text{O}} = \ln \gamma_{\text{O}}^0 + \left(\frac{\partial \ln \gamma_{\text{O}}}{\partial X_{\text{O}}}\right)X_{\text{O}} + \frac{1}{2}\left(\frac{\partial^2 \ln \gamma_{\text{O}}}{\partial X_{\text{O}}^2}\right)X_{\text{O}}^2 + \dots + \frac{1}{n!}\left(\frac{\partial^n \ln \gamma_{\text{O}}}{\partial X_{\text{O}}^n}\right)X_{\text{O}}^n \dots \quad (12)$$

where γ_{O}^0 is independent of the oxygen concentration in the alloy. In LBE, the atom fraction is always very small, i.e., $X_{\text{O}} \ll 1$. Then the interactions among the oxygen atoms can be neglected, or the higher order terms of X_{O} in Eq. 12 can be omitted. For such cases, the activity coefficient γ_{O} is independent on the oxygen concentration and $\gamma_{\text{O}} \approx \gamma_{\text{O}}^0$.

Another chosen standard state for oxygen activity is often the saturation state, and the activity of oxygen in LBE for such a standard state can be calculated as:

$$a_{\text{O}}^* = \frac{X_{\text{O}}}{X_{\text{O},s}} = \frac{\gamma_{\text{O}}}{(P_{\text{O}_2,s})^{1/2}} X_{\text{O}} = \gamma_{\text{O}}^* X_{\text{O}} \quad (13)$$

where $X_{\text{O},s}$ and $(P_{\text{O}_2,s})^{1/2}$ are the saturation oxygen atom fraction in the alloy and the corresponding partial pressure.

Experimental results of oxygen activity in liquid lead-bismuth alloys are scarce compared to those in pure liquid lead and bismuth. Taskinen [59] measured the oxygen activity in lead-bismuth alloys in the temperature range from 1073-1173 K. By adding bismuth up to 55% atom fraction, the effects of bismuth on oxygen activity were examined. Otsuka et al. [60] examined the entire range of lead-bismuth alloy compositions at 1073 K. Anik and Froberg [61] examined the thermodynamics of oxygen in lead-bismuth alloy at 1173 K. Comparisons between the theoretical and experimental results can be found in Ref. [57].

4.2. Solubility and diffusivity of oxygen in LBE

The solubility of oxygen in LBE is a function of temperature and can be expressed as [62]:

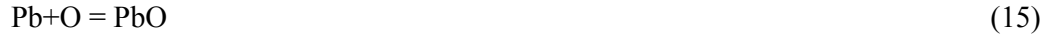
$$\log C_{\text{O}}[\text{wt}\%] = 1.2 - 3400/T[\text{K}], \quad (14a)$$

in temperature range of 400 – 700°C. Alternatively, for the solubility expressed in atomic percent (mole fraction):

$$\log X_{\text{O}}[\text{at}\%] = 2.3 - 3400/T[\text{K}]. \quad (14b)$$

The solubility of oxygen in pure liquid lead was measured by Szwarc et al. [63], Alcock and Bedford [64], and Charle and Osterwald [65], and the solubility in pure liquid bismuth was measured by Fitzner [66], Hahn and Stevenson [67], and Heshmatpour and Stevenson [68]. Comparisons between the solubility of oxygen in lead, bismuth, and LBE are shown in Fig. 9. Most of the LBE corrosion test facilities are operated in the temperature range of $623\text{K} < T < 823\text{K}$. Fig. 9 indicates that the solubility of oxygen in LBE is greater than that in pure lead and bismuth in this temperature range.

The oxygen partial pressure in equilibrium with oxygen saturated in LBE can be calculated through the equilibrium of the following reaction in LBE:



At equilibrium

$$\Delta F_{\text{PbO}} = -RT \ln\left(\frac{a_{\text{PbO}}}{a_{\text{O}} a_{\text{Pb}}}\right) = -RT \ln\left(\frac{a_{\text{PbO}}}{P_{\text{O}_2}^{1/2} a_{\text{Pb}}}\right), \quad (16)$$

where ΔF_{PbO} [J/mol] is the standard free energy of formation of the oxide. The free energy is a function of temperature and can be found from the oxide handbook [69].

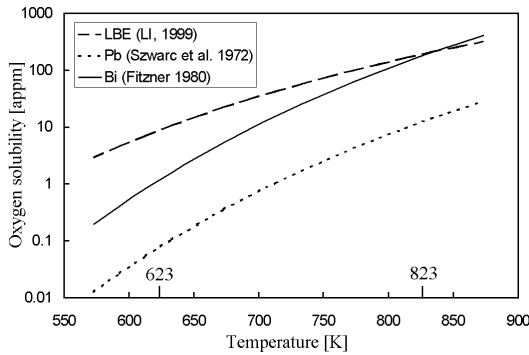


FIG. 9. Oxygen solubility in LBE, lead, and bismuth.

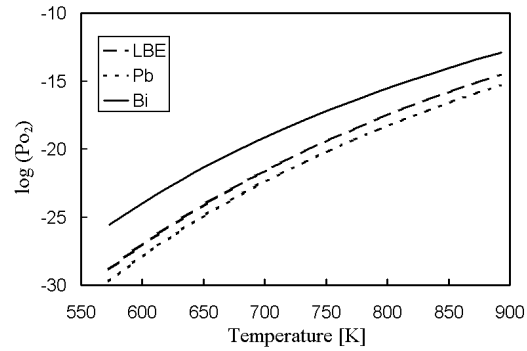


FIG. 10. Oxygen partial pressure in equilibrium with saturated oxygen, in LBE, lead, and bismuth.

When oxygen is saturated, PbO precipitates from the eutectic and its activity becomes unity, that is $a_{\text{PbO}} = 1$. The saturation partial pressure of oxygen is expressed as:

$$P_{\text{O}_2,s} = a_{\text{Pb}}^{-2} \exp\left(\frac{2\Delta F_{\text{PbO}}}{RT}\right). \quad (17)$$

Correspondingly, the oxygen partial pressure in equilibrium with oxygen saturated in pure liquid lead and pure liquid bismuth can be expressed as:

$$P_{O_2,s(Pb)} = \exp\left(\frac{2\Delta F_{PbO}}{RT}\right) \text{ and} \quad (18)$$

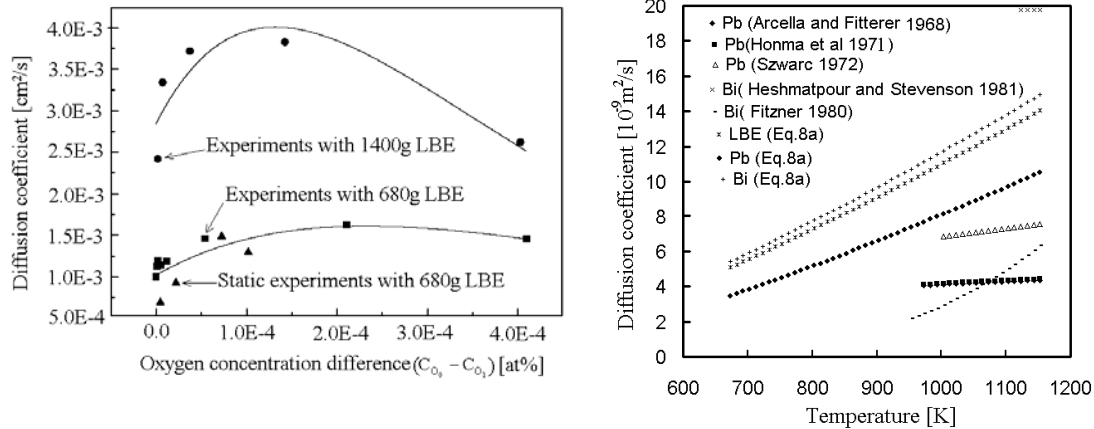
$$P_{O_2,s(Bi)} = \exp\left(\frac{2\Delta F_{Bi_2O_3}}{3RT}\right). \quad (19)$$

Temperature dependence of the oxygen partial pressure for saturated liquid lead, bismuth, and LBE is shown in Fig. 10, which indicates that the difference between the oxygen partial pressure for LBE and that for lead is small. Since the difference is due to the different activities of lead in pure lead and in LBE, the assumption of Li [55] that the activity of lead in LBE is unity is reasonable. Knowing the oxygen partial pressure and saturation concentration, the activity coefficient of oxygen in LBE can be calculated as $\gamma_O = P_{O_2,s}^{1/2} / X_{O,s}$. Based on Eqs. 16 and 17, the activity of PbO can be expressed as:

$$a_{PbO} = \frac{a_O}{a_{O's}} = \frac{X_O}{X_{O,s}} = \frac{C_O}{C_{O,s}}, (X_O, C_O \ll 1) \quad (20)$$

Another important property for oxygen in LBE is the mass diffusion coefficient. To our best knowledge, there is no experimental correlation for this diffusion coefficient. The only reported measurement of this coefficient was conducted by Lefhalm et al. [70].

The dependency of the oxygen diffusion coefficient on the oxygen concentration difference and the different LBE masses (ratio surface/volume) at 430°C is shown in Fig. 11a [70]. The results indicated that the coefficient is around $10^{-7} \text{ m}^2/\text{s}$ and depends on ratio between surface and volume and the oxygen concentration.



(a) Dependence of diffusion coefficient on concentration difference for different LBE masses (ratio surface/volume) at 430°C, with C_{O_0} = initial concentration and C_{O_1} = final concentration [70].

(b) Oxygen diffusion coefficient in LBE, liquid lead, and liquid bismuth with temperature.

FIG. 11. Oxygen diffusion coefficient in LBE, lead, and bismuth.

However, for the diffusion coefficients of oxygen in pure liquid lead and bismuth, there are several correlations, such as in Refs. [63,71,72] for lead, and in Refs. [66,68] for bismuth. Figure 11b shows the oxygen diffusion coefficients in LBE, lead, and bismuth from Eq. 8a and the various experimental correlations. Except for the data from Ref. [68], the calculated values are greater than the measured values. Eq. 8a predicts a value of a diffusion coefficient around $10^{-8} \text{ m}^2/\text{s}$, more than an order of magnitude smaller than that from Ref. [70].

4.3. Oxygen Control System

The oxygen control technique developed in Russia [55,62] promotes the formation of protective oxide layers on steel surfaces to prevent direct dissolution of metals and oxide precipitation in the eutectic by carefully controlling the oxygen concentration in LBE. Based on Eq. 17, to prevent the precipitation of PbO , the oxygen partial pressure must satisfy the criterion $RT \ln P_{\text{O}_2} < 2\Delta F_{\text{PbO}} - 2RT \ln a_{\text{Pb}}$. To obtain the needed partial pressure for forming the protective oxide layer based on Fe_3O_4 , we assume that the following reaction occurs at steel surfaces at equilibrium:



then we get:

$$\Delta F_{\text{Fe}_3\text{O}_4} = -RT \ln \frac{a_{\text{Fe}_3\text{O}_4}}{a_{\text{O}}^4 a_{\text{Fe}}^3}, \quad (22)$$

Iron is the main composition of the steels that are used for containment of LBE, then it is reasonable to set $a_{\text{Fe}} \approx 1$, and $a_{\text{Fe}_3\text{O}_4} = 1$ for continuous films. To form a solid protective oxide layer, the oxygen partial pressure must satisfy $RT \ln P_{\text{O}_2} = RT \ln a_{\text{O}}^2 > 1/2\Delta F_{\text{Fe}_3\text{O}_4}$. Therefore, for LBE the oxygen partial pressure should be controlled in the range:

$$1/2\Delta F_{\text{Fe}_3\text{O}_4} < RT \ln P_{\text{O}_2} < 2\Delta F_{\text{PbO}} - 2RT \ln a_{\text{Pb}}, \quad (23)$$

For pure liquid lead, the activity of Pb is unity, i.e. $a_{\text{Pb}} = 1$. Then

$$1/2\Delta F_{\text{Fe}_3\text{O}_4} < RT \ln P_{\text{O}_2} < 2\Delta F_{\text{PbO}}. \quad (24)$$

For pure lead and LBE, Eqs. 23 and 24 indicate the lower limits of the oxygen partial pressure for forming the protective oxide layer are the same. The only difference between the upper limits is the term related to the Pb activity. The limit of the oxygen partial pressure (equaling the saturation partial pressure) is shown in Fig. 10. The figure indicates that the activity of Pb in LBE has little influence on the partial pressure. In fact, in the right-hand side of Eq. 23, the second term containing the activity of lead in LBE is much smaller than the first term. Based on Eqs. 16 and 20, we obtain the relation between the oxygen concentration and the oxygen partial pressure as:

$$\ln P_{\text{O}_2} = 2(\ln C_{\text{O}} - \ln C_{\text{O},s}) + 2\Delta F_{\text{PbO}} / RT - 2 \ln a_{\text{Pb}}, \quad (25)$$

Therefore, the oxygen concentration in LBE should be kept in the range:

$$C_{\text{O},s} a_{\text{Pb}} \exp\left(\frac{\Delta F_{\text{Fe}_3\text{O}_4} - 4\Delta F_{\text{PbO}}}{4RT}\right) < C_{\text{O}} < C_{\text{O},s}, \quad (26)$$

or equivalently oxygen activity of oxygen in LBE should be kept in the range:

$$a_{\text{Pb}} \exp\left(\frac{\Delta F_{\text{Fe}_3\text{O}_4} - 4\Delta F_{\text{PbO}}}{4RT}\right) < a_{\text{O}}^* < 1, \quad (27)$$

The upper and lower limits of oxygen concentration in LBE and liquid lead are shown in Fig. 12. One way to control the oxygen level is to control the oxygen partial pressure using cover gas systems such as $H_2/O_2/H_2O$ and $CO/O_2/CO_2$. The former is particularly attractive since the hydrogen can be used to reduce PbO contaminant as well [73]. In the $H_2/O_2/H_2O$ system, at the stable state, the oxygen partial pressure can be calculated as:

$$P_{O_2} = \left(\frac{P_{H_2O}}{P_{H_2}}\right)^2 \exp\left(\frac{2\Delta F_{H_2O}}{RT}\right). \quad (28)$$

Therefore, the oxygen partial pressure is determined through controlling the ratio of the partial pressures of H_2O and H_2 . According to Eq. 23, P_{H_2O}/P_{H_2} should be controlled in the range:

$$1/4\Delta F_{Fe_3O_4} - \Delta F_{H_2O} < RT \ln(P_{H_2O}/P_{H_2}) < \Delta F_{PbO} - \Delta F_{H_2O} - RT \ln a_{pb}, \quad (29)$$

The upper and lower limits of the ratio P_{H_2O}/P_{H_2} are shown in Fig. 13, as well as the constant oxygen concentration lines. In the typically operating temperature range ($350^\circ\text{C} \sim 550^\circ\text{C}$) of an LBE loop, the maximum oxygen concentration in LBE is the saturation concentration at 350°C , which is 5.5×10^{-5} wt%, corresponding to $P_{H_2O}/P_{H_2} = 10^{3.13}$; the minimum oxygen concentration is the minimum concentration that the magnetite film can form at 550°C which is 7.19×10^{-9} wt%. Taking into account all of these, the reasonable ratio P_{H_2O}/P_{H_2} in the cover gas of a non-isothermal LBE loop with an operating temperature range ($350^\circ\text{C} \sim 550^\circ\text{C}$) can be determined (gray area in Fig. 13).

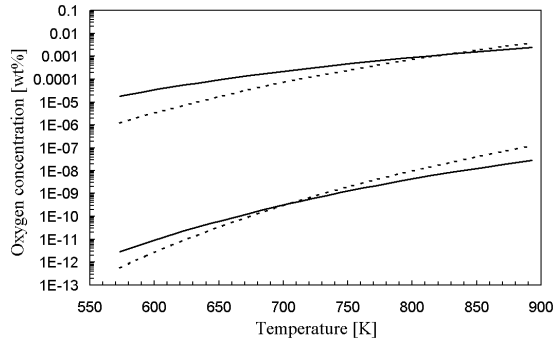


FIG. 12. Upper and lower limits of oxygen concentration in LBE (solid lines) and pure lead (dashed lines)

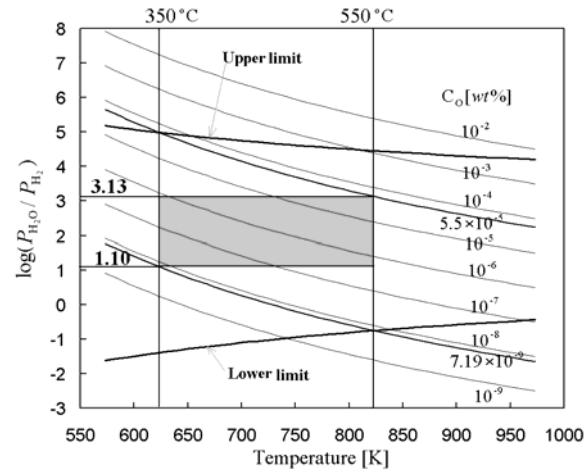


FIG. 13. H_2 and H_2O mixture in the cover gas for controlling oxygen level. The thick lines are the upper and lower limits of P_{H_2O}/P_{H_2} . The thin lines are for constant oxygen concentration. The typical operating temperature range for LBE loop and the reasonable partial P_{H_2O}/P_{H_2} are shown in the gray area. $C_O[\text{wt}\%] = 5.5 \times 10^{-5}$ is the saturated oxygen concentration at 350°C ; $C_O[\text{wt}\%] = 7.19 \times 10^{-9}$ is the lowest oxygen concentration for forming magnetite film at 550°C .

Another simple graphic illustration of the proper oxygen control parameters is to draw the Ellingham diagram that contains oxygen potentials of the relevant oxides PbO , NiO , Fe_3O_4 ,

and Cr_2O_3 and the lines for constant oxygen partial pressures and constant $P_{\text{H}_2\text{O}} / P_{\text{H}_2}$ ratios as a function of temperature. Such a diagram, demonstrating in which region the stable conditions exist and how they can be established, was given in Ref. [74] for pure lead system. Taking into account of the activity of lead in LBE, the refined Ellingham diagram for LBE was given in Ref. [75].

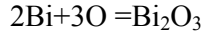
4.4. Oxygen Sensor

Several types of oxygen sensors are underdevelopment [76-80] for measuring the oxygen level in LBE. In electrochemical terms, the sensor can be represented by the following equation:



where superscript prime denotes the reference, and the solid electrolyte is typically yttrium-stabilized zirconium (YSZ, $\text{ZrO}_2\text{--Y}_2\text{O}_3$). For fixing the oxygen activity or partial pressure of the reference, pure oxygen ($P'_{\text{O}_2} = 1$) or air ($P'_{\text{O}_2} = 0.21$, the standard state is pure O_2 at 1 atmosphere) as gas reference or metal/metal oxide buffers such as $\text{In}/\text{In}_2\text{O}_3$, $\text{Bi}/\text{Bi}_2\text{O}_3$, Sn/SnO_2 , $\text{Cu}/\text{Cu}_2\text{O}$ and many others so-called coexistence electrodes of that types have been used worldwide [77]. The reference electrode of $\text{Bi}/\text{Bi}_2\text{O}_3$ with saturated oxygen has been used successfully in Russia [7,55], and such sensors are under development and testing in lead-alloy coolant technology development program at Los Alamos National Laboratory [80]. Therefore, we will limit the analysis to such a sensor. For analysis on other types of sensors ($\text{In}/\text{In}_2\text{O}_3$, Sn/SnO_2 , Pb/PbO), refer to Refs. [76,77,79].

In the reference electrode, the reaction is:



For the equilibrium state, the oxygen partial pressure can be expressed as:

$$(P'_{\text{O}_2})^{1/2} = a'_{\text{O}} = \exp\left(\frac{\Delta F_{\text{Bi}_2\text{O}_3}}{3RT}\right), \quad (30)$$

At the working electrode, the oxygen partial pressure can be calculated using Eq. 16. The electrochemical potential $E(\text{V})$ is:

$$E = \frac{RT}{2F} \ln\left(\frac{P'_{\text{O}_2}}{P_{\text{O}_2}}\right)^{1/2} = \frac{1}{2F} \left(\frac{1}{3} \Delta F_{\text{Bi}_2\text{O}_3} - \Delta F_{\text{PbO}} - RT \ln a_{\text{PbO}} + RT \ln a_{\text{Pb}}\right), \quad (31)$$

where F is the Faraday constant. Substituting Eq. 20 into Eq. 31, we get

$$C_{\text{O}} = C_{\text{O},s} \exp\left[\frac{1}{RT} (-2FE + \frac{1}{3} \Delta F_{\text{Bi}_2\text{O}_3} - \Delta F_{\text{PbO}}) + \ln a_{\text{Pb}}\right], \quad (32a)$$

and by setting $a_{\text{Pb}} = 1$, we get:

$$C_{\text{O}} = C_{\text{O},s} \exp\left[\frac{1}{RT} (-2FE + \frac{1}{3} \Delta F_{\text{Bi}_2\text{O}_3} - \Delta F_{\text{PbO}})\right], \quad (32b)$$

Therefore, from the EMF reading of the oxygen sensor, we can determine the oxygen concentration level in LBE.

To form the protective oxide layer and to prevent the precipitation of lead oxide, the real value of the sensor should be in the following range:

$$\frac{RT}{2F} \left(\frac{\Delta F_{\text{Bi}_2\text{O}_3}}{3RT} - \frac{\Delta F_{\text{PbO}}}{RT} + \ln a_{\text{Pb}} \right) < E < \frac{RT}{2F} \left(\frac{\Delta F_{\text{Bi}_2\text{O}_3}}{3RT} - \frac{\Delta F_{\text{Fe}_3\text{O}_4}}{4RT} \right), \quad (33)$$

The maximum of the sensor corresponding to the minimal oxygen level in LBE that can form the iron oxide (Fe_3O_4) and the minimum of the oxygen sensor corresponding to saturated oxygen.

Corresponding to the Ellingham diagram, the A-C-T-E (activity-concentration-temperature-EMF) diagram can be drawn based on the above equations. Such diagrams for liquid lead and LBE are given in Ref. [81]. The A-C-T-E thermodynamic equilibrium diagram for a specific sensor in LBE/lead can be used as an instrument for control, analysis, and diagnostics of technological and corrosion processes in a non-isothermal circulation system [81].

The refined (including the effects of the lead activity in LBE) A-C-T-E diagram for Bi/ Bi_2O_3 oxygen sensor is given in Fig. 14. From this figure, it is easy to determine the regime in which the oxygen sensor signal should be to form the protective Fe_3O_4 film and prevent the precipitation of lead oxides.

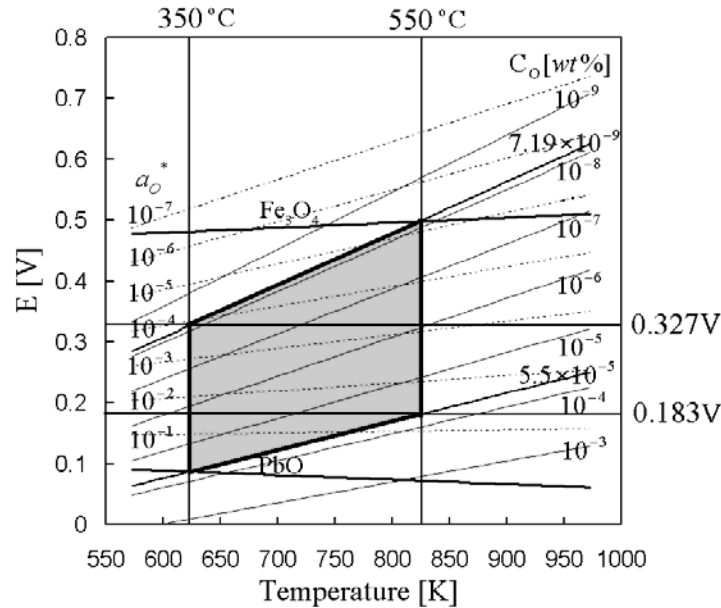


FIG. 14. A-C-T-E diagram for oxygen in LBE. The operating temperature range for typical LBE systems and nominal oxygen sensor output range are shown in the gray area. The activity of lead in LBE is taken into account for the calculations.

5. Overview of Experimental Results

Early experimental results on the corrosion of steels in LBE with or without inhibitors were well summarized in a previous review [52]. Here, we focus on the recent experimental results on steels exposed to flowing and static LBE with or without oxygen control. The chemical compositions of tested steels are given in Table 2.

TABLE 2. Chemical compositions of the tested materials (wt%)

Material	Cr	Ni	Mo	Mn	V	Nb	W	Ti	Si	C
1.4970 wt%	16.5	13.8	0.66	1.91	—	—	—	—	0.89	0.46
316L wt%	17.3	12.1	2.31	1.8	—	—	—	—	0.35	0.02
Manet II wt%	10.3	0.68	0.61	0.78	0.2	0.14	—	—	—	0.11
Manet	10.3	0.68	0.61	0.78	—	—	—	—	—	0.11
Optivier Iv c	9.1	—	—	0.52	0.22	—	1.4	—	—	0.12
EM10 wt%	9.0	0.1	1.0	0.5	—	—	—	—	0.3	0.1
T91 wt%	8.26	0.13	0.95	0.38	0.2	0.075	—	—	0.43	0.105
Batman 28	8.94	0.05	0.01	3.51	0.24	0.01	1.51	0.01	0.32	0.09
Batman 27	9.0	0.07	0.01	3.1	0.21	0.01	1.45	0.2	0.49	0.1
EP823	12	0.8	0.9	0.8	0.4	0.4	0.8	—	1.3	0.18
F82H	7.75	0.015	0.01	0.16	0.14	<0.01	—	0.004	0.23	0.1
Mod 9Cr-1Mo	8.41	0.06	0.88	0.4	0.2	—	0.0005	0.005	0.3	0.1
T-410	12.5	0.34	—	1	—	—	—	—	1	—
EP302	16	10	—	0.8	—	1	—	—	3	0.12
HT9	11.5	0.5	—	0.6	—	—	—	—	0.4	—
D9	17	12	—	2	—	—	—	—	1	—
Mod F82H	7.8	0.04	—	0.18	0.16	<0.01	2	0.01	0.13	0.09
410ss	12.2	0.12	0.02	0.8	0.07	—	—	0.01	0.067	0.067
430ss	16.24	0.15	0.02	0.23	0.1	—	—	0.01	0.52	0.08
JPCA	14.14	15.87	2.29	1.54	0.03	—	0.01	0.22	0.5	0.058
2.25Cr-1Mo	2.18	0.02	0.92	0.44	0.01	—	—	0.01	0.34	0.1
F82H	7.72	0.02	<0.01	0.01	0.18	—	1.95	0.005	0.1	0.095

5.1. Ferritic/Martensitic Steels

Corrosion tests of martensitic steels (IVc, T91, Batman 27 and 28, EP823, EM10) in flowing LBE with a velocity about 2 m/s were carried out in an LBE loop at two temperatures (573 and 743 K) for 1000, 2000, and 3000 hours [82]. The oxygen level is about 10^{-6} wt%. No dissolution of steel components was found. The thickness of the protective oxide layer increases with increasing temperature and exposure time. Except for Batman 27 and 28, the oxide generally consists of two layers (Fig. 15), with a porous outer layer (mainly Fe_3O_4) and a compact inner layer [mainly spinel $(\text{Fe,Cr})_3\text{O}_4$].

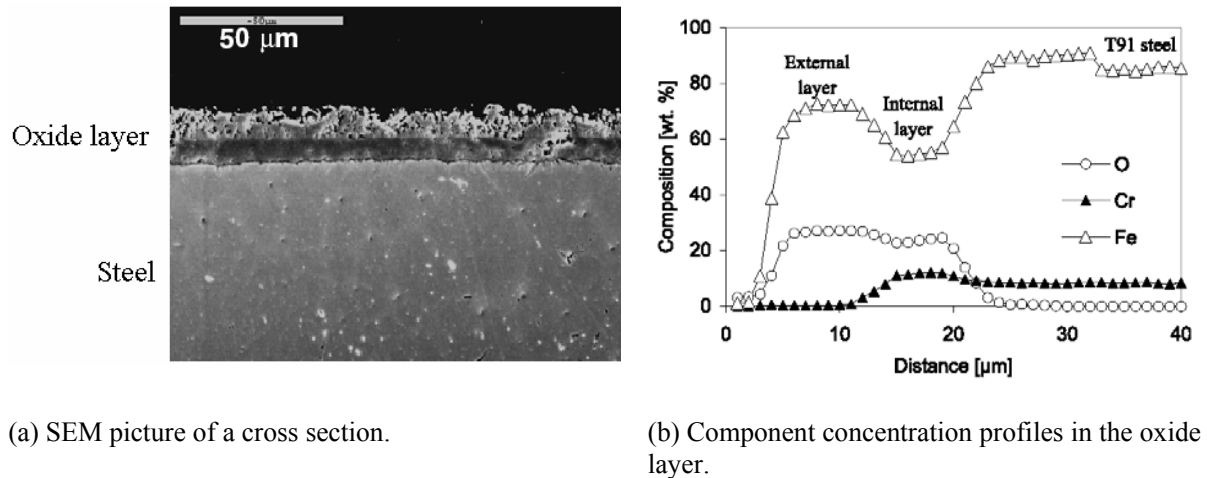


FIG. 15. Oxide structure of T91 steel after exposing to flowing LBE 3000 hours [82]. Experimental conditions are 743 K, 2 m/s LBE velocity and 0.01 ppm oxygen level. The oxide layer for such steel consists of two zones, a porous outer layer (mainly Fe_3O_4) and a compact inner layer [mainly spinel $(\text{Fe,Cr})_3\text{O}_4$].

For Batman 27 and 28, an oxygen dissolution layer is found beneath the inner oxide layer. The oxide layer thickness depends on the composition of the steel. It is found that the thickness is ordered as the following: EP823<BA27<T91<BA28<EM10<IVc, indicating that a high level of silicon in the steel can enhance the oxidation resistance.

The oxidation processes of IVc and EM 10 steels in flowing pure lead were also examined in Ref. [83] at 673 K and 823 K with an oxygen level of $3 - 4 \times 10^{-5}$ wt% for 3000 hr. The lead velocity is 2 m/s. The oxide layer can reach 30 μm at 823 K that is much greater than that in Ref. [82] for the same exposure time. Except for the double-layer oxide, an oxygen diffusion layer was also observed for both EM10 and IVc steels. Still the thickness of all three zones (two oxide zones and one oxygen diffusion zone) formed on EM10 steel is smaller than on IVc steel. The oxide layer is effective in preventing the dissolution of the steel components.

At 873 K, T91 and EM10 steels were tested for 1000 h in flowing LBE with an oxygen concentration of 10^{-6} wt% at 743 and 873 K [84]. At 873 K, comparing to the results from test below 823 K, the thick oxide layer (20 to 25 μm) consists of three zones: the outer zone is Fe-Cr spinel and the inner zone is an oxygen diffusion zone, the intermediate zone is localized observed and appears porous and heterogeneous and its thickness varies. Decreasing the oxygen level to 10^{-7} - 10^{-8} wt%, the oxide layer becomes thinner and the intermediate zone disappears, while the composition of the oxide layer is similar to that of high oxygen levels. Weight losses were also observed.

Tests of T91 steel were also carried out at oxygen level between 3.1×10^{-10} and 7.3×10^{-8} wt% in the LECOR loop at 673 K [85]. The oxygen level is too low to form the oxide layer on the sample surface. So even at such low temperature, dissolution and cavities were observed. Weight change measurements indicate that the corrosion rate is about 0.0029 $\mu\text{m}/\text{h}$. Liquid metal penetration was detected.

Corrosion tests of MANET steel were carried out in static LBE at 573, 673, and 749 K [86] and 573, 673, and 823 K [87] at saturated oxygen up to 5000 hr. At 573 and 673 K. The oxide layer has similar composition with those of other martensitic steels tested in flowing LBE and the steel did not suffer any dissolution corrosion attack. While at 823 K, the MANET steel specimens exposed to LBE exhibited liquid metal corrosion, and the liquid metal penetration into the bulk of the steel was more severe with increasing exposure time. Besides the dissolution of the steel elements and the penetration of the LBE into the steel, thin oxide scales were detected in a few places.

Experimental results on MANET steel in flowing LBE with a velocity of 2 m/s were reported at 693 and 823 K with an oxygen level of 10^{-6} wt% [88]. At 823 K, an effective protective oxide layer was formed and no steel element dissolution was found unlike the behaviors in the static tests in Ref. [87]. In the static tests, oxygen reaches the steel surface through diffusion that is very slow. Therefore, it is possible that dissolution has already started before an oxide layer can form at higher temperatures. In flowing LBE, oxygen can quickly reach the surface through convection and the conditions favor the formation of the protective layer.

Short-term (100 and 665 h) static corrosion tests of F82H-mod steel samples with or without pre-oxidation were carried out at 673 and 873 K [89]. For low oxygen concentrations in LBE, dissolution of the samples without pre-oxidation occurs and the pre-oxidation does not prevent materials dissolution in time after the oxide film decomposes. For high oxygen concentrations, pre-oxidation improves the feasibility of the protective oxide layer formed in

LBE conditions. The oxide layer observed on the pre-oxidation sample surface was quite homogeneous, non-permeable to LBE comparing to that on the sample without pre-oxidation.

F82H-mod samples were also tested in a natural convection loop at 773 K and a beginning oxygen level of 0.06 ppm for different exposure times [90]. The results indicate that sustaining a pre-formed oxide layer needs a smaller oxygen concentration than that for forming a new oxide layer on smooth steel surfaces. At an oxygen level between 0.003 and 0.004 ppm, it was found that the temperature threshold for protective oxide layer formation was around 823 K for F82Hmod steel in static LBE. Above 823 K, corrosion (dissolution) occurs and the formation of the protective oxide layer is impossible [91].

Corrosion tests of HT-9 and T410 were carried out at 460 and 550°C with oxygen concentration of 0.03-0.05 wppm and flow velocity of 2 m/s [92,93]. For HT-9 steel specimens, double-layer oxide films formed on the steel surfaces and no dissolution was observed after 3000 hours at 550°C. While for T410 steel specimens, only spinel oxide films formed and the films were not uniform, and heavy dissolution occurred even at the lower temperature (460°C). At 460°C, the thickness of the film on HT-9 is 1-8, 12-14 and 14-16 μm after 1000, 2000, and 3000 hours of tests, respectively. At 550°C, the thickness reaches an average value of 38 μm with some patches reaching 44 μm after 3000 hours [92].

5.2. Austenitic Steels

Austenitic steels have more Cr and Ni than martensitic steels. Corrosion tests of AISI 316L and 1.4970 steels were carried out in flowing LBE at an oxygen level of 0.01 ppm at 573 and 743 K [82]. A very thin oxide layer (Fig. 16) on the steel surfaces was found on specimens after 3000 hours. Other tests of 1.4790 steel indicated that the thin oxide layer could also form at 643 K in flowing LBE with a velocity of 2 m/s at an oxygen concentration of 0.01-0.02 ppm in 3116 hr tests [94]. X-ray maps and concentration profiles show that there are not any changes in the distribution of steel elements, indicating that the thin film ($<<1$ μm) can protect steels against dissolution corrosion.

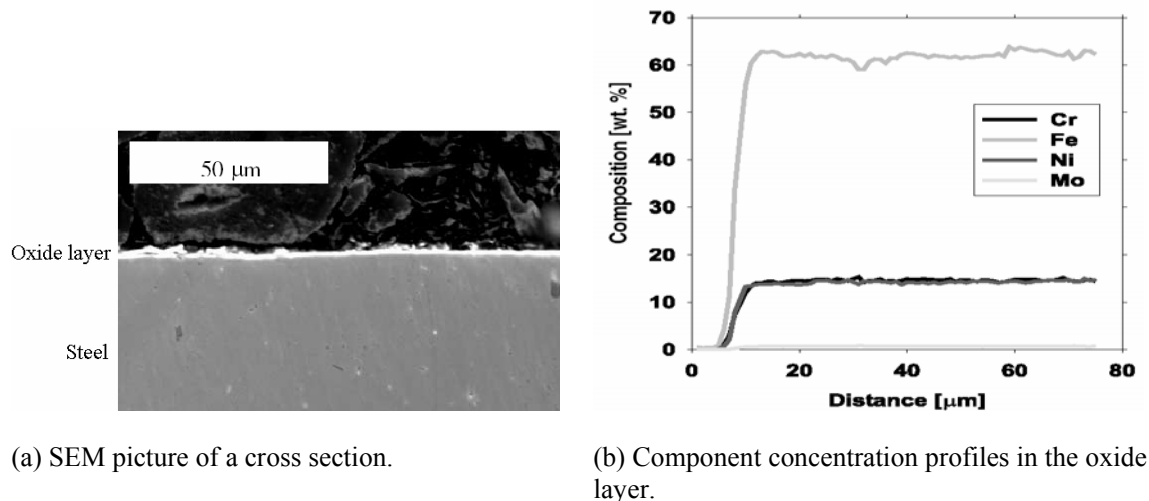


FIG. 16. Oxide structure of steel 1.4970 after exposure to flowing LBE 3000 hours [82]. The experimental conditions are 743 K, 2 m/s LBE velocity, and 0.01 ppm oxygen level. The oxide layer of such steels is much thinner than that of T91 steel under the same conditions.

Corrosion tests of 316L steel were carried out in flowing LBE with a velocity of 2 m/s and an oxygen level of 0.01ppm at 823 K up to 2000 hours [88]. A double-layer oxide film formed on the steel surfaces similar to the oxide structure on martensitic steel surfaces, and no dissolution was observed [88], indicating that the double-layer oxide film can also protect the austenitic steel against dissolution at 823 K. Increasing the temperature to 873 K, deep liquid metal penetration and massive ablation of material by erosion were observed. Tests of 1.4970 steel with the same condition showed that a continuous magnetite scale with a spinel zone underneath formed on surfaces and precipitation of the chromium was observed at the grain boundary at both 823 K and 873 K [88]. If the steel was surface-alloyed by Al forming FeAl, no dissolution was observed even at 873 K for both 1.4970 and 316L steels.

Corrosion attack of AISI 316L is reported at 873 K under two oxygen levels of 0.01 ppm and 0.001ppm [84]. For very low oxygen levels ($< 7.3 \times 10^{-4}$ ppm), even at a low temperature of 673 K, weight loss was found for AISI 316L samples after 1500 h of test. The dissolution rate is estimated 1.52×10^{-5} mg/mm²h that is less than that of martensitic steel (T91) under the same conditions [85].

Corrosion tests of AISI 316L in static LBE were carried out up to 1500, 3000, and 5000 hr [87]. The oxygen concentration was at saturation limit. At the lower temperatures (573 and 673 K), thin oxide layers formed on steel surfaces similar to the test results in flowing LBE at low temperatures, and no dissolution was found. While at 823 K, the steels were attacked by LBE and there were significant dissolution of alloy elements. Corrosion tests of 316L and 316 steels were carried out simultaneously at 460 and 550°C with oxygen concentration of 0.03-0.05 wppm and flow velocity of 2 m/s [92,93]. At the lower temperature of 460°C, thin spinel oxide films formed on both steels and no dissolution corrosion was observed. At the higher temperature of 550°C, for 316L steel, a double-layer oxide film formed, similar to that from other experiments in flowing LBE [84] and no dissolution was observed after 3000 hours, while for 316 steel, the oxide film still has the single-layer structure and significant dissolution was observed similar to the experimental results in static LBE [87]. D-9 steel was also tested under the same conditions [92]. Its behaviors at 460 and 550°C were similar to those of 316L except that the oxide thickness was much thicker than that of 316L steel at 550°C.

5.3. Oxidation Kinetics

For long-term operation, it is expected that the oxidation of steels in LBE follows the following law similar to that of steels in air:

$$\delta = K_{\delta} t^n = A \exp(-Q/RT) t^n, \quad (34)$$

where δ and t are the thickness of the oxide film and the time, respectively, K_{δ} is the oxidation rate constant depending on steel compositions and operation conditions, A is a constant depending on materials and environment, Q is an activation energy, n is a constant depending on the oxidation mechanism.

For lower temperatures, such as $T < 500^{\circ}\text{C}$, it has been reported that $n = 1/2$, i.e., the oxide film growth follows a parabolic law. Measured oxide layer thickness growth in time for some martensitic steels was fitted using the parabolic law at $T = 470^{\circ}\text{C}$ [82]. The results indicate that the oxidation rate depends strongly on steel compositions. Other tests [92] of martensitic steels (HT-9, T-410) and austenitic steels (D-9, 316L) also indicate that oxide layer thickness growth in time follows the parabolic law.

With increasing temperature, the constant n in Eq. 34 is expected to vary for different materials due to the complex kinetics. To determine the time dependence of oxidizing different materials in liquid metal, Gorynin et al. [56] correlated their experiments results of several steels in flowing lead using Eq. 34 (Fig. 17).

According to Wagner's theory, the parabolic rate constant K_p of steel oxidation in gas can be calculated as [95]:

$$K_p = \int_{P_{O_2}^I}^{P_{O_2}^{II}} \left(\alpha \frac{D^*(M)}{f_M} + \frac{D^*(O)}{f_O} \right) d[\ln P_{O_2}], \quad (35)$$

Where $P_{O_2}^I$ and $P_{O_2}^{II}$ are oxygen partial pressure at oxide/metal and oxide/gas interface, respectively, M denotes the metal, D^* and f are the trace self-diffusion coefficient and the correlation factors, respectively, α is the molar ratio of oxygen to metal in the oxide. For example, for magnetite Fe_3O_4 , Eq. 35 becomes to [96]:

$$K_p(Fe_3O_4) = \frac{4}{3} \int_{P_{O_2}^I}^{P_{O_2}^{II}} \frac{D^*(Fe)}{f_{Fe}} d[\ln P_{O_2}] \quad (36)$$

In Eq. 36, the diffusion coefficient of oxygen through the magnetite film is neglected because it is much smaller than the diffusion coefficient of iron through the oxide film. The value of f_{Fe} is approximately 0.5 when transport occurs by a vacancy mechanism and in the range of 0.4-1 for mechanism involving interstitials [97].

Equations 35 and 36 have been successfully used in the oxidation of metals in gas. They are expected to be applicable in the oxidation of steel in liquid metals/alloys with slight modification through taking into account the dissociation of the oxide at the oxide/LBE interface. In Ref. [92], Eq. 35 was employed to calculate the parabolic rate constant of steel in flowing LBE at 550°C. Although the dissolution did not take into account, the calculated oxide thickness agreed very well with the experimental results.

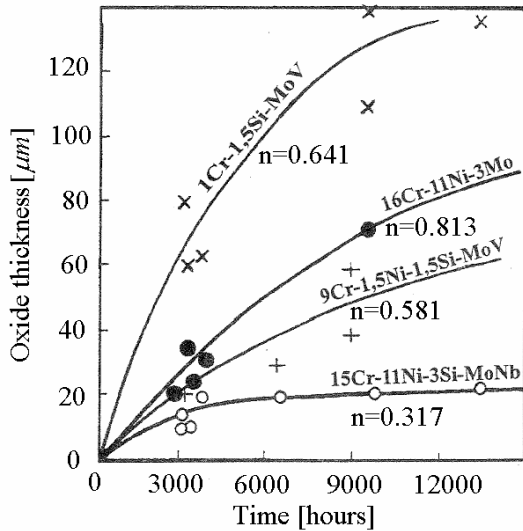


FIG. 17. Oxidation kinetics of the martensitic steels tested at 470°C in flowing lead [56].

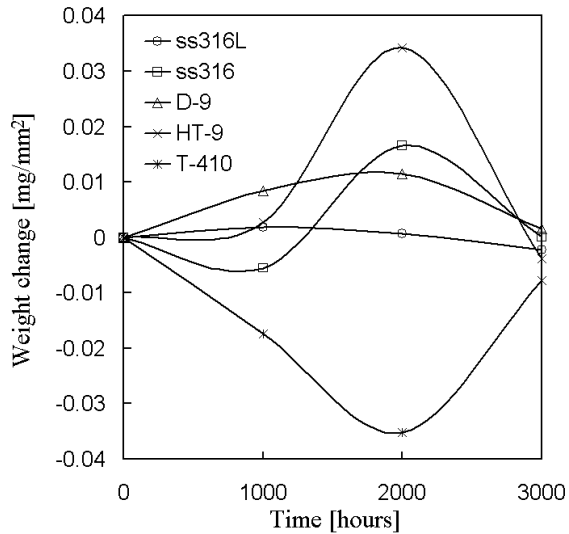


FIG. 18. Weight changes of U.S. steels tested in flowing LBE with velocity of 2 m/s and oxygen concentration of 0.03-0.05 ppm at 550°C [92].

A direct measure of the simultaneous oxidation and dissolution of steels in LBE is the weight change. Studies of some U.S. steels (HT-9, T-410, 316L/316, and D-9 [92,93]) at 460°C indicate that weight changes of the all the steel specimens approximately follow the parabolic law. At 550°C, except for T-410 steel which was subjected significant erosion, the characteristics of the weight changes of other steels in the first 2000 hours of testing period is very different from that afterwards (Fig. 18 [92]).

When steels are exposed to LBE with oxygen control, oxidation and dissolution of the alloying components occur simultaneously. The oxidation leads to a weight gain, while the dissolution results in a weight loss. If the two processes are diffusion limited, the weight change should follow a parabolic law. Unlike the case in air, it is expected that the oxide thickness can reach to a plateau in LBE. When the oxide film reaches this balanced state, the oxidation rate at the substrate equals the dissociation rate at the oxide/LBE interface. At 550°C, the oxidation process dominates the whole process initially, and it reaches a turning point at around 2000 hours. After that the weight change turns downwards because the weight loss due dissociation/dissolution begins to manifest. At 460°C, the initial oxidation process may not have completed in 3000 hours due to the much slower kinetics at the lower temperature.

5.4. Summary of the experimental results

The above analysis indicates that the experimental results of steels in LBE are very scattered, however we can make some general conclusions based on these results:

- For very low oxygen levels ($<10^{-4}$ ppm), both austenitic and martensitic steels in LBE are subjected to dissolution even at temperatures as low as 673 K. The dissolution rate of an austenitic steel is less than that of a martensitic steel.
- In the temperature range of 573 to 743 K, protective oxide films can form on austenitic and martensitic steel surfaces at oxygen levels above 10^{-4} ppm. The thin oxide films can protect the steel elements against rapid dissolution of steel components into LBE. The protective layer for martensitic steels is much thicker than that for austenitic steels..
- Generally, the oxide films on martensitic steel have a double-layer structure: an outer porous layer of magnetite and an inner compact layer of Fe-Cr spinel. The films grow at both interfaces: the LBE/oxide interface and the oxide/steel interface. The oxide films on austenitic steel surfaces are mostly composed of Fe-Cr spinel at lower temperatures.
- At 823 K, dissolution is observed for AISI 316L steel in static LBE with saturated oxygen, while double-layer oxide films were found in flowing LBE.
- For temperatures above 823 K, heavy dissolution corrosion of austenitic steels occurs. These steels cannot be used without special treatments. If the steel surface is alloyed with Al to form FeAl alloy or treated using the GESA method, a protective oxide layer can form even at 873 K. Although durability of such protective films is good for the test durations of a few thousand hours, it is not clear that they can be self-healing if failures occur.
- For martensitic steels, very thick oxide films form on the surfaces if the temperature is above 823 K. This indicates that long-term applications of these steels in their original states may be problematic since thick oxides are not very protective and will become unstable.
- Between 750 K and 823 K, a transition temperature or temperature range exists in which the corrosion mechanism changes from oxidation to dissolution. It is possible to form the protective oxide layer on steel surfaces. The corrosion behaviors depend on the steel compositions, the steel surface treatment, the oxygen concentration in LBE, etc.

6. Corrosion Modeling Results

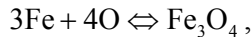
Although corrosion tests of steels in LBE have been carried out for both static and flowing conditions, the data is still too limited for applications to practical coolant systems. In addition, most of the recent experimental studies only focused on the oxidation process due to relatively short test durations. In practice, two processes (dissolution and oxidation) occur simultaneously at the steel surfaces in contact with LBE with oxygen control. Because the existing tests are only up to a few thousands hours, the weight losses are not well captured due to more rapid oxidation in the early times.

Another important phenomenon is the deposition of corrosion products in a practical coolant loop. The deposition in the cooler areas of a coolant loop may lead to severe flow restriction and microstructure changes in the materials, and could destroy the flow system eventually. However, most of the existing test loops are designed for corrosion tests. Knowledge on deposition is very scarce compared to corrosion.

Precise simulation of all conditions encountered in practical applications can be very expensive and time consuming. Therefore, developing corrosion/precipitation models to predict the corrosion/precipitation behaviors in practical coolant loops and to properly apply the limited experiment results becomes very important in lead-alloys coolant technology development.

6.1. Corrosion Behaviors at Interface

For systems with oxygen control, the oxygen is transported by both diffusion and convection to steel surfaces. At the beginning, oxidation and dissolution may occur simultaneously. If the oxidation process is favored and dominates, protective oxide films form on the steel surface. Once the oxide films form, the direct dissolution is reduced significantly because the film separates the steel surface from LBE. For such cases, iron diffuses through the oxide layer (Fig. 19), and formation or dissociation of magnetite occurs at the oxide/LBE interface (assuming that the oxide contacting with LBE is magnetite) at the same time. With increasing time, the oxide layer becomes thicker and the diffusion rate of iron through the oxide layer becomes smaller because of the increasing thickness. The following reaction reaches equilibrium state at the interface:



Then we get:

$$a_{\text{Fe}} = \frac{1}{a_{\text{O}}^{4/3}} \exp\left(\frac{\Delta F_{\text{Fe}_3\text{O}_4}}{3RT}\right), \quad (37)$$

where the activity of iron equals $C_{\text{Fe}} / C_{\text{Fe},s}$ according to the Henry's law. For turbulent flows, it is reasonable to assume that the oxygen concentration is uniform in the system and the reaction between oxygen and lead in LBE (Eq. 15) is at equilibrium locally, then we get:

$$a_{\text{O}} = \frac{a_{\text{PbO}}}{a_{\text{Pb}}} \exp\left(\frac{\Delta F_{\text{PbO}}}{RT}\right). \quad (38)$$

From Eq. 20, we obtain the relation between the Fe concentration (the main corrosion product) and the oxygen concentration in LBE at the steel surface:

$$C_{Fe} = C_{Fe,s} a_{pb}^{4/3} \left(\frac{C_{O,s}}{C_O} \right)^{4/3} \exp \left[\frac{1}{3RT} (\Delta F_{Fe_3O_4} - 4\Delta F_{PbO}) \right]. \quad (39a)$$

If the oxide contacting with LBE is Cr_2O_3 or NiO , the surface concentration of Cr or Ni can be calculated as:

$$C_{Cr} = C_{Cr,s} a_{pb}^{3/2} \left(\frac{C_{O,s}}{C_O} \right)^{3/2} \exp \left[\frac{1}{2RT} (\Delta F_{Cr_2O_3} - 3\Delta F_{PbO}) \right], \quad (39b)$$

$$C_{Ni} = C_{Ni,s} a_{pb} \left(\frac{C_{O,s}}{C_O} \right) \exp \left[\frac{1}{RT} (\Delta F_{NiO} - \Delta F_{PbO}) \right]. \quad (39c)$$

Equation 39a-39c is valid when a continuous oxide layer can form. On the other hand, the corrosion product concentration at the surface should be smaller than its saturation concentration, i.e., $C_M / C_{M,s} < 1$, otherwise, Eq. 6 should be employed for the surface concentration.

For mass transfer controlled corrosion at the steady state, the surface corrosion product concentration is calculated by using either Eq. 6 or Eq. 39 depending on the oxygen concentration in LBE. Eqs. 6 and 39 indicate that the corrosion product concentration at the interface is a function of temperature and oxygen concentration. The dependency of the concentration on temperature and oxygen concentration are shown in Fig. 20. The concentration increases with temperature and it can be reduced significantly through increasing the oxygen concentration in LBE. It needs to be pointed out that a higher oxygen concentration leads to a very thick oxide layer and more severe oxidation corrosion. In a practical LBE coolant system, both the liquid metal (dissolution) and oxidation corrosion should be controlled. It is expected there exists an optimal oxygen concentration range in which a proper oxide film can form to minimize total corrosion.

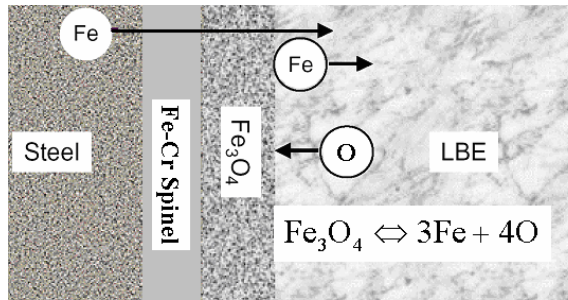


FIG. 19. Corrosion dynamics at the interface. Oxide layer forms at the steel/LBE interface.

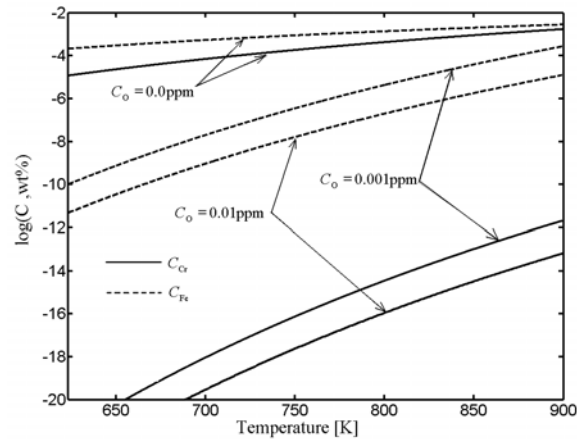


FIG. 20. Corrosion product concentration at oxide/ LBE interface of mass transfer controlled corrosion.

For a practical nuclear coolant loop, the temperature can be expressed as a function of the axial position of the loop. Therefore the surface corrosion product concentration is a function of the axial coordinate in a non-isothermal loop. If the activity of lead in LBE is set to unity, Eq. 39 reduces to the equation obtained by Li [55] based on equilibrium between lead and magnetite at steel surfaces.

6.2. Kinetic Corrosion Model (mass transfer controlled)

A kinetic corrosion model for mass transfer controlled corrosion was developed based on solving the mass transport equation in the boundary layer [50,98]. The kinematic viscosity of LBE is much greater than the diffusion coefficient of corrosion products in LBE. The Schmidt number is very high ($Sc = \nu / D$, where ν is the kinematic viscosity), so the corrosion product transport is controlled by mass transfer through a thin boundary layer. By making some reasonable assumptions, the convection and diffusion equation in the mass transfer boundary layer is simplified as [50,98]:

$$\gamma \frac{\partial c}{\partial x} = D \frac{\partial^2 c}{\partial y^2}. \quad (40)$$

The meaning and units of all variables in Eq. 40 are same to these in Ref. [98]. c [wppm] is the corrosion product concentration, x [m] and y [m] are coordinates in the axial and transverse directions, respectively, γ [1/s] is the wall shear rate and it is constant along the simple loop here and can be calculated by $\gamma = \lambda V^2 / 2\nu$ (λ is the Fanning friction factor). The surface concentration c_w of the corrosion product is expanded in the following Fourier series:

$$c_w = \sum_k c_k \exp(2\pi k \xi), \quad (41)$$

where ξ is the non-dimensional axial coordinate ($\xi = x / L$, L is the loop length). The solutions for the concentration in the boundary layer and the flux of the corrosion product from (corrosion) or to (precipitation) to the pipe wall are:

$$c = c_0 + \sum_{k>0} Y_k(\eta) e^{2\pi k i \xi} + \sum_{k<0} \bar{Y}_{|k|}(\eta) e^{2\pi k i \xi}, \quad (42)$$

$$q = \left(\frac{2\pi D^2 \gamma}{3L} \right)^{1/3} \frac{1}{\Gamma(1/3)} \sum_{k \neq 0} Q_k \exp(2\pi k i \xi), \quad (43)$$

where $Y_{k>0}(\eta) = \frac{c_k}{Ai(0)} Ai((2\pi k i)^{1/3} \eta)$ and $Y_{k<0}(\eta) = \bar{Y}_{|k|}(\eta)$ (the overbar denotes conjugate),

$Q_{k>0} = \frac{c_k}{Ai(0)} k^{1/3} i^{1/3}$ and $Q_{k<0} = \frac{c_k}{Ai(0)} |k|^{1/3} (-i)^{1/3}$, Ai and Γ are Airy Function and Gamma

Function, respectively, and η is defined as $\eta = \left(\frac{\gamma}{DL} \right)^{1/3} y$.

Equation 43 can be used to predict the corrosion/precipitation rate profile in non-isothermal simple liquid metal loops. Equation 43 has been extended to solutions that can be applied to multi-modular loops [99] and the transient corrosion/precipitation process [100]. Some observed corrosion phenomena (such as “down-stream” effects) are naturally included.

In the bulk flow, the transport process of the corrosion product in flowing liquid metal satisfies the following convective mass transfer equation:

$$\frac{d[c_b A(x) V(x)]}{dx} = p(x) q[\xi(x)], \quad (44)$$

where A [m²] is the flow area and p [m] is the perimeter, For circular tubes, $A = \pi d^2 / 4$ and $p = \pi d$ (the boundary layer thickness is neglected because it is much smaller than the hydraulic diameter), c_b [wppm] is the corrosion product concentration in the bulk. For simple loop systems, A , p and V are constant along the axis, the solution of c_b for simple loop was given as [101]:

$$c_b(\xi) = c_b^0 + \frac{4d}{V} \frac{(2\pi L^2 D^2 \gamma)^{1/3}}{3^{1/3} Ai(0) \Gamma(1/3)} \sum_k P_k \exp(2\pi k i \xi), \quad (45)$$

where c_b^0 is the average bulk concentration and equals the average surface concentration a_0 at the steady state, $P_0 = 0$, $P_{k>0} = Q_k / (2\pi k i)$ and $P_{k<0} = \overline{P_{k>0}}$ (the over bar denotes conjugate). For multi-modular loop systems, A , p and V are functions of the axial coordinate x , while the volume flow rate $Q = A(x)V(x)$ is constant. The bulk concentration can be calculated using the following integration [99]:

$$c_b(x) = \frac{1}{Q} \int_0^x F[x(s)] p[x(s)] q(\xi[x]) ds + c_b(0), \quad (46)$$

where $c_b(0)$ is the bulk concentration at $\xi = 0$ and can be calculated by $c_b(0) = c_b(L)$.

6.3. Kinetic corrosion model (activation controlled)

In Refs. [98-101], it is assumed that the liquid lead-alloys corrosion is mass transfer controlled. Therefore the surface corrosion product concentration is specified using Eq. 6 or 39, depending on the oxygen level in LBE. Most of the studies performed in liquid metals are limited to such type of corrosion. However, in case of very high flow velocity, the mass transfer rate is much higher than the dissolution at the steel surface and rate-determining step is dissolution, i.e. the corrosion is activation controlled.

For activation controlled corrosion, it is expected that the corrosion product concentration at surface equals to that in the bulk. At the steady state, the bulk concentration in a non-isothermal liquid metal simple loop satisfies:

$$Q \frac{dc_b(x)}{dx} = p(x) \kappa_d(x) [C_{eq}(x) - c_b(x)], \quad (47)$$

where C_{eq} is the equilibrium concentration determined by Eq. 6 or Eq. 39, κ_d is the dissolution rate of steel components or the oxide, and it can be expressed as [41]: $\log \kappa_d = A_\kappa + B_\kappa / T$ (A_κ and B_κ are constants).

A general solution of Eq. 48 was given in Ref. [41]:

$$c_b(x) = e^{-\phi(x)} [I(x) + G], \quad (48)$$

$$\text{where } \phi(x) = \int \frac{p(x)}{Q} \kappa_d(x) dx, \quad I(x) = \int \frac{p(x)}{Q} \kappa_d(x) C_{eq}(x) e^{\phi(x)} dx, \quad (49)$$

G is an integral constant and can be found from the fact that $c_b(0) = c_b(L)$.

If the bulk concentration is expanded into a Fourier series, the solution for Eq. 48 becomes:

$$c_b(x) = \sum_k \frac{b_k(1 - 2\pi k i / l)}{1 - 4k^2 \pi^2 / l^2} \exp[2\pi k i \phi(x) / l], \quad (50)$$

where $l = \int_0^L \frac{p(x)}{Q} \kappa_d(x) dx$ and the constant b_k is the harmonics of the Fourier transform of

$$C_{eq}(x) : C_{eq}(x) = \sum_k b_k \exp[2\pi k i \phi(x) / l].$$

The corrosion/precipitation rate in a non-isothermal closed loop for activation controlled corrosion is calculated as:

$$q(x) = \kappa_d(x) \sum_k \frac{b_k(2\pi k i / l - 4\pi^2 k^2 / l^2)}{1 - 4\pi^2 k^2 / l^2} \exp[2\pi k i \phi(x) / l]. \quad (51)$$

To calculate the corrosion/precipitation rate for activation controlled corrosion, the dissolution rate of steel components (low oxygen concentration case) or the dissociation rate of the oxide in contact with LBE should be specified. However, to our best knowledge, there is no report on such rates in existing literatures.

6.4. Improving the Local Corrosion Models

For mass transfer controlled corrosion, the corrosion rate can be simply written as:

$$q = K(c_w - c_b), \quad (52)$$

where c_w is the surface concentration, K [m/s] is the mass transfer coefficient depending on the local conditions (local liquid velocity, local temperature, etc.). Several mass transfer coefficient expressions have been developed in aqueous media based on the experimental data [102-104]:

- Berger and Hau [102]: $K_{B-H} = 0.0165 \nu^{-0.530} D^{0.670} V^{0.860} d^{-0.140}$,
- Silverman [103]: $K_{Silverman} = 0.0177 \nu^{-0.579} D^{0.704} V^{0.875} d^{-0.125}$,
- Harriott and Hamilton [104]: $K_{H-H} = 0.0096 \nu^{-0.567} D^{0.654} V^{0.913} d^{-0.087}$.

The bulk concentration c_b in Eq. 52 is unknown. For an isothermal pipe flow, c_b is always assumed to be zero or equals to the concentration at the inlet. Balbaud-Celerier and Barbier [44] applied the local models to liquid metal loops. They predicted a corrosion rate 2.4 times higher than the experimental results. It was believed that the assumption of a zero bulk concentration was one important reason leading to such a high prediction.

For non-isothermal liquid metal loops without a protective layer, Epstein [41] improved the application of the local model by assuming that the bulk corrosion product concentration equals the saturated concentration at the coldest leg and the surface concentration at the hottest leg equals the local saturated concentration. Then the gradient between the bulk concentration and the hot leg surface concentration can be expressed as:

$$c_w - c_b = C_{M,s,h} - C_{M,s,c} \frac{dC_{M,s}}{dT} \Delta T, \quad (53)$$

where M denotes the corrosion product, h and c denote the hot and cold legs, respectively, and ΔT is the difference between the maximal and the minimal temperatures. Then the corrosion rate at the hot section can be calculated by [41]:

$$q_{T_{\max}} = K \frac{dC_{M,s}}{dT} \Delta T. \quad (54)$$

Taking into account the total amount of corrosion equals to the total amount of precipitation in the entire loop, Zhang and Li [51] improved application of local models to steel corrosion in LBE loops through assuming a constant corrosion product concentration in the bulk:

$$c_b = \frac{\int_0^L K(x)c_w(x)dx}{\int_0^L K(x)dx}. \quad (55)$$

The corrosion/precipitation profile can be calculated by [51]:

$$q(x) = \frac{K(x)}{\int_0^L K(x)dx} [c_w(x) - \int_0^L K(x)c_w(x)dx], \quad (56)$$

For calculation, it is assumed that $K(x)$ is the local mass transfer rate depending on only the local conditions.

If it is assumed that the mass transfer rate $K(x)$ is a known function, then the corrosion product in the bulk flow follows the following the equation for the simple loop:

$$\frac{\partial c_b(x,t)}{\partial t} + V \frac{\partial c_b(x,t)}{\partial x} = \frac{4}{d^2} [d - 2\delta(x)] K(x) [c_w(x) - c_b(x,t)], \quad (57)$$

where $\delta(x)$ is the mass transfer boundary layer thickness and can be calculated by $\delta(x) = D(x)/K(x)$. The initial condition of Eq. 57 can be set as $c_b(x, t=0) = 0$. The solution to Eq. 57 is:

$$c_b(x,t) = \sum_k \frac{a_k(1 - 2\pi k i V / l)}{1 - 4\pi^2 k^2 V^2 / l^2} (1 - \exp[-(1 + V/l)\psi(x)]) \exp[2\pi k i \psi(x)/l], \quad (58)$$

where $\psi(x) = \int \frac{4}{d^2} [d - 2\delta(x)] K(x) dx$ and $l = \int_0^L \frac{4}{d^2} [d - 2\delta(x)] K(x) dx$.

The corrosion/precipitation rate based on the local corrosion model for varying bulk concentration at the steady state can be expressed as:

$$q(x) = K(x) \sum_k \frac{a_k(2\pi k i V / l - 4\pi^2 k^2 V^2 / l^2)}{1 - 4\pi^2 k^2 V^2 / l^2} \exp[2\pi k i \psi(x)/l], \quad (59)$$

6.5. Sanier and Santarini model

Sanier and Santarini [105] developed a corrosion model for non-isothermal liquid metal loop by dividing the corrosion process into three steps: convection in the bulk flow, diffusion in the boundary layer and dissolution at the interface.

$$\text{Convection rate in the bulk flow: } q = \frac{\rho d V}{4\rho_0} \frac{dc_b}{dx}. \quad (60)$$

$$\text{Dissolution rate at the interface: } q = \frac{K_d}{C_{M,s}} (C_{M,s} - c_w). \quad (61)$$

$$\text{Diffusion rate through the boundary layer: } q = \frac{\rho D}{\rho_0 \delta} (c_w - c_b). \quad (62)$$

In Eqs.60-62, ρ is the liquid metal density and varies along the axial direction, ρ_0 is the density of the dissolved metal and is constant through the loop, K_d is the dissolution rate defined as: $K_d = K_{d0} \exp(-Q_d / RT)$. δ is the boundary layer thickness and assumed to be constant through the loop. In Ref. [105], the solubility of metal M $C_{M,s}$ and the diffusion coefficient D are expressed as: $C_{M,s} = C_{M,0} \exp(-Q_C / RT)$ and $D = D_0 \exp(-Q_D / RT)$. The total amount of corrosion equals to the total amount of precipitation:

$$\int_0^L q(x) dx = 0. \quad (63)$$

Case 1: activation controlled ($V = \infty$, $D = \infty$):

$$C_b = C_w, \quad q = K_{d0} \exp(-\frac{Q_d}{RT}) - \frac{K_{d0}}{C_{M,0}} c_b \exp(\frac{Q_C - Q_d}{RT}). \quad (64)$$

Case 2: diffusion controlled ($V = \infty$, $K_d = \infty$):

$$C_w = C_{M,s}, \quad q = \frac{\rho D_0 C_{M,0}}{\rho_0 \delta} [\exp(-\frac{Q_D - Q_C}{RT}) - \frac{c_b}{C_{M,0}} \exp(-\frac{Q_D}{RT})], \quad (65)$$

Case 3: convection controlled ($D = \infty$, $K_d = \infty$):

$$C_w = C_{M,s}, \quad q = \frac{\rho D_0 C_{M,0} Q_C}{4 \rho_0 R T^2} \frac{dT}{dx} \exp(-\frac{Q_C}{RT}). \quad (66)$$

Case 4: Mixing control:

$$\frac{d[(C_{M,s} / K_d + \rho_0 \delta / \rho D) q]}{dx} + \frac{4 \rho_0}{\rho D V} q - \frac{dC_{M,s}}{dx} = 0, \quad (67)$$

In all the cases, the bulk concentration is calculated using Eq. 63.

6.6. Comparisons between Modeling and Experimental Results

Experimental results of corrosion tests performed in a non-isothermal simple lead loop were reported [105]. The oxygen level is assumed very low. The diameter of the tube is 0.0247 m. The highest temperature in the loop is 550°C (at the test leg) and the lowest temperature is 465°C. The flow velocity is 0.115m/s. Experiments were carried at three locations in the test leg. The corrosion depth for 10CD 9-10 steel was between 110, 100, and 75 μm after 3000 hours, and between 40, 25, and 30 μm after 2800 hours for Z 10 CD Nb V 92 steel.

Balbaud-Celerier and Barbier [44] employed the local corrosion model (Eq. 52) to calculate the corrosion rate in the pure lead loop. The bulk concentration of Fe was assumed to be zero. The calculation gave a value around 240 μm per 3000 hours that is 2.4 times larger than the experiments results.

By assuming that the bulk concentration equaled the solubility of Fe at the coldest leg, Epstein [41] obtained an expression for the corrosion rate at the hottest leg in a non-isothermal closed loop (Eq. 54). We apply Eq. 54 to the pure lead loop and obtain a corrosion rate of 182 μm per 3000 hours. The calculated value is still much larger than the experimental results. In Zhang and Li's [51] improved local model (Eq. 56), the bulk concentration was

also assumed to be constant, but it was calculated based on the fact that the total amount of corrosion equals to the total amount of precipitation in non-isothermal close loops. Using Eq. 56, it is found that the predicted corrosion rate is around 93 μm per 3000 hours agreeing very well with the experimental results.

The above calculations using the local and improved local models show that the corrosion rate at the highest temperature leg depends strongly on the corrosion product bulk concentration. The models give reasonable corrosion rates considering there are uncertainties in many factors: the value of the diffusion coefficient and the surface concentration, effects of the materials composition and erosion, etc. However, the improved local corrosion model can only give a constant corrosion rate at the highest temperature leg.

The corrosion/precipitation profile in the entire pure lead loop from the kinetic corrosion model (Eq. 43) is show in Fig. 21, as well as the results from Eq. 67 (Sanier and Santarini's model) and Eq. 59 (improved local model with varying bulk concentration along the loop axis). In the calculations from Eq. 67, the parameters in Ref. [105] are selected. It is assumed that the mass transfer rate $K = D / \delta = K_1 \exp(K_2 / RT)$.

Using the selected values of K_1 , K_2 , $C_{m,0}$, and Q_C (Ref. [105]), Eqs. 59 and 67 give almost the same profile, and corrosion rates at the test section are consistent with the experimental results. However, the selected mass transfer coefficients and the Fe solubility in lead are very different from the correlations [40,102-104] obtained experiments.

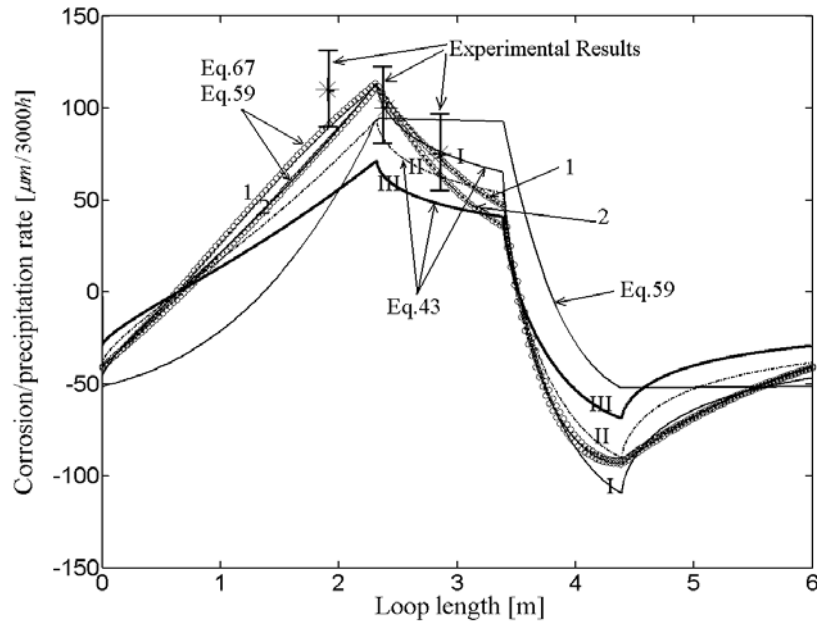


FIG. 21. The corrosion/precipitation profile in the entire lead loop and comparisons between the different model results and the experiment results from Ref. [105]. I: $D = 3.9 \times 10^{-9} \text{ m}^2/\text{s}$, II: $D = 2.9 \times 10^{-9} \text{ m}^2/\text{s}$ and III: $D = 1.9 \times 10^{-9} \text{ m}^2/\text{s}$ are from Eq. 43. 1: $K_1 = 0.566 \text{ m/s}$, $K_2 = 45.2 \text{ kJ}$, $Q_C = 25.1 \text{ kJ}$, $C_{M,0} = 3.06 \text{ ppm}$, 2: $K_1 = 0.0322 \text{ m/s}$, $K_2 = 27.6 \text{ kJ}$, $Q_C = 58.6 \text{ kJ}$, $C_{M,0} = 238 \text{ ppm}$, from Eq. 59 (circles) and Eq. 67 (solid line). $D[\text{m}^2/\text{s}] = 4.9 \times 10^{-7} \exp(-44100 / RT)$ is used in the solid curve from Eq. 59. A positive value of the rate corresponds to corrosion and a negative value to precipitation.

Employing the mass transfer coefficient expression developed by Berger and Hau [102] and diffusion coefficient expression developed by Robertson [43], Eq. 59 can only give the corrosion and precipitation zone and cannot give the location where the highest corrosion/precipitation occurs.

Based on experimental results, the diffusion coefficient of Fe in pure lead is around $10^{-9} \text{ m}^2/\text{s}$. For the calculations, three values $(1.9, 2.9, 3.9) \times 10^{-9} \text{ m}^2/\text{s}$ were selected for comparison. The surface concentration is calculated using the experimental correlation from Ref. [40]. Figure 21 shows that the kinetic model predicted results agreeing very well with the experimental results. Since the kinetic corrosion model is based on the assumption that corrosion rate is controlled by the mass transfer rate through the boundary, we conclude that the corrosion process in this particular pure lead loop is mass transfer controlled.

A LBE loop called JLBL-1 loop [106] was set up in the Japan Atomic Energy Research Institute (Japan). Some initial experiments have been carried out to study the corrosion and deposition without active oxygen control (Fig. 22). The entire loop in contact with LBE is made of stainless steel 316 (SS316). The inner diameter of the circulating tube, the test tube at the low temperature, and that at high temperature is 22, 22, and 10 mm, respectively. The flow velocity is 1 m/s in the hot test tube and 0.2 m/s in the other parts. The oxygen concentration was not measured during the experiment and no oxide film was reported. The corrosion depth was less than 0.1 mm per 3000 hours in the high temperature test tube. Since there is no oxide layer reported, it is assumed that the corrosion process is due to direct dissolution. Because there is variation of the flow cross-section along the loop, the kinetic corrosion model for multi-modular loop [99] is applied to calculate the corrosion/precipitation profile in JLBL-1 loop.

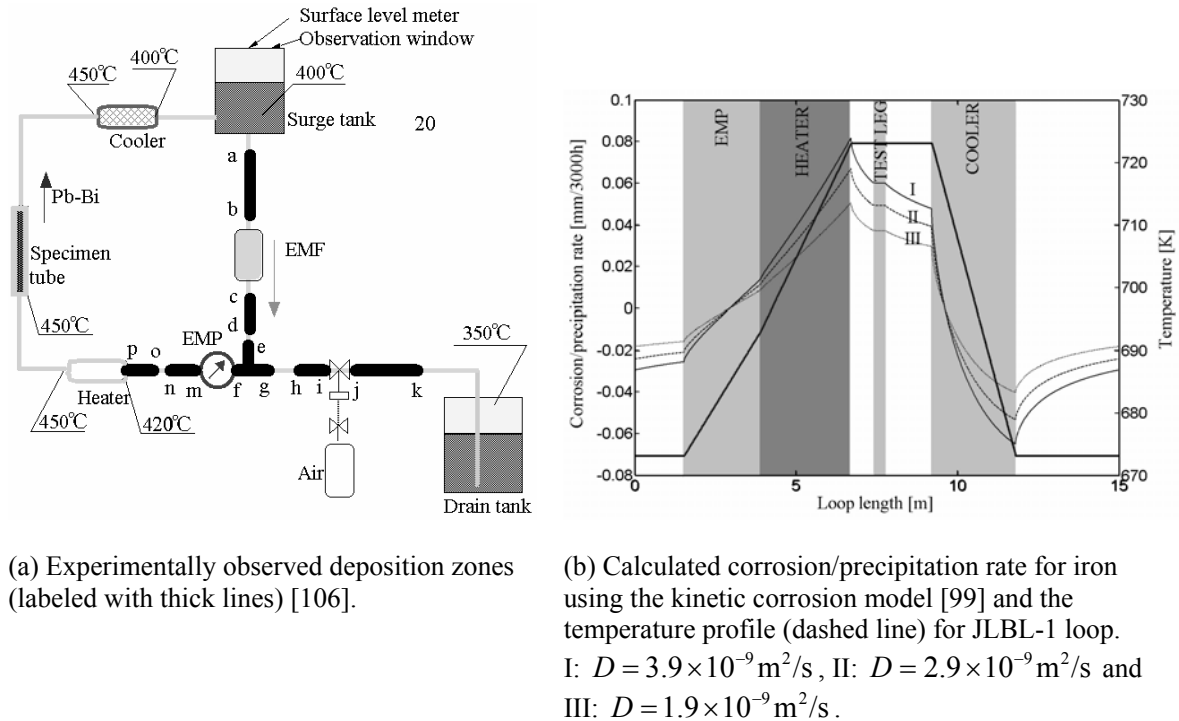


FIG. 22. Experimental and modeling results for JLBL-1 loop.

The calculated pure iron corrosion/precipitation profile for the JLBL-1 loops shows that the observed deposition zones in the JLBL-1 loop can be exactly predicted using the present non-isothermal and multi-modular corrosion model. The predicted corrosion rate is about 0.05-0.08 mm per 3000 hours if the diffusion coefficient is selected as $3.9 \times 10^{-9} \text{ m}^2/\text{s}$. This agrees well with experimental results of 0.03~0.1 mm.

6.7. Erosion-Corrosion

For high velocity flows or flow at high temperatures, the strong shear stress may strip the protective oxide films or the deposited corrosion product, causing erosion-corrosion. Slot erosion of 316L and T-410 steels in flowing LBE at 550°C was reported in Ref. [92]. The depth and length of erosion of 316L were 120-140 and 820 μm , under conditions with a flow velocity 2 m/s and an oxygen concentration 0.03-0.05 ppm. The depth and length of slot erosion of T-410 under the same conditions are 80 μm and 60 mm, respectively. Erosion phenomena were also reported in Ref. [84] for T-91 and 316L steels in flowing LBE at 873 K.

The erosion-controlled rate is much higher than the mass transfer controlled corrosion rate and increases dramatically with flow velocity (Fig. 7). To our best knowledge, there is no modeling study on erosion induced by the heavy liquid metal flow. Erosion models for corrosion fouling, especially on the removal of the deposits, were developed by Bartlett [107], Charlesworth [108] and recently reviewed by Somerscales [109]. The erosion models in fluidized-bed were well reviewed by Lyczkowski and Bouillard [110]. For practical applications in coolant system, it is important to understand and verify the on set of erosion, and design away from it.

7. Recommended Subjects for Further Studies

Recently, numerous experimental and theoretical studies on LBE coolant technology and materials have been carried out worldwide. Substantial amount of useful information for designing practical LBE nuclear coolant systems has been obtained. However, there are still significant gaps and the existing results can not provide a high fidelity correlation of the corrosion rate to factors influencing the corrosion processes in LBE coolant systems. To fill these technical gaps before the LBE nuclear coolant technology is ready for programmatic and industrial applications, the following aspects need to be further studied.

7.1. Precipitation and Deposition of Corrosion Products

In practical nuclear coolant LBE loops, corrosion products from the hot legs are transported to some other locations and deposited. It is precipitation and deposition that sustain corrosion in non-isothermal LBE loops during long-term operations. Deposition has a positive feedback mechanism and may lead to severe flow restrictions, which results in increased pump power requirement and eventual flow blockage. Although deposition plays important roles in non-isothermal LBE loops, measurement of deposition rate and distribution is very scarce. Most of the present test loops are built for corrosion tests. Therefore, systematic studies of precipitation, deposition, and development of mitigation strategies and methods should be carried out.

7.2. Oxygen Transport

In oxygen controlled LBE systems, the oxygen dissolved in LBE is transported to the steel surface to form, sustain and restore protective oxides through convection and diffusion. Because the chemical reaction is fast in the operating temperature range, the oxygen mass

transport determines the process kinetics. To understand the mass transport process of the dissolved oxygen, it is necessary to know the diffusion coefficient and the transport properties of oxygen in LBE. This is particularly important in large and/or natural convection systems. Transport models, measurement facilities, and controlling technology should be developed. The optimal oxygen levels and the reliable operation of oxygen control systems should be determined and developed.

7.3. Oxide formation and kinetics in lead-alloys

The oxidation mechanisms and kinetics for steels in LBE are not well understood at the present. The oxide growth kinetics should be determined through analysis of the experimental data. However, the available data is not sufficient to provide correlations covering the desired design space between the oxide growth and the operating conditions, especially their dependency on temperature and oxygen concentration. More experiments are needed, both short- and long-durations. Theoretical models should be developed, incorporating the dissolution effects at the oxide/LBE interface (which differentiate oxidation in lead-alloys from oxidation in air), to interpret and apply the limited experimental data. Since protection by oxide is a key feature in lead-alloy coolant technology, and long-term corrosion is via interaction through the oxide, this subject is of critical importance.

7.4. Coolant hydrodynamic effects

Coolant flow can accelerate mass transfer of corrosion products and result in higher corrosion rates. It can also transport oxygen quickly to the interface to form and restore protective oxides. However, the flow effects on the oxide formation and dissolution are still not well understood on fundamental and quantitative levels that would lead to sound prediction based on limited test results. The other uncertainty is erosion due to high or erratic flow, exacerbated by the high density of heavy metal coolants. There are no experimental data and theoretical analysis on erosion and corrosion-erosion in LBE non-isothermal loops. In sections where flow changes direction abruptly and where there are vortices, the flow effects will be more pronounced and should be studied carefully and mitigated accordingly.

7.5. Steel Composition, Microstructure and Surface Effects

According to experimental results on austenitic and martensitic steels, the oxide characteristics are closely dependent on the compositions of steels. But that dependency is not well understood to more precisely guide the selection and development of suitable materials. Experiments on a variety of steels in static or flowing LBE should be carried out, with emphasis on Cr and Si effects. There is also experimental evidence that the initial surface condition may affect the subsequent oxide growth and protectiveness. The preferential transport and dissolution of certain alloy compositions can also change the microstructure of the materials in the long run and may lead to materials failures. These effects need to be investigated, and practical solutions sought for enhanced corrosion resistance while preserving radiation damage resistance.

7.6. Corrosion Models

Although the final selection and verification of materials with adequate corrosion resistance have to be based on testing in near-prototypic conditions, it is nonetheless extremely valuable to develop proper corrosion models for the design and interpretation of tests and application of test data to design and prediction of system performance. It was found from the present kinetic model for loops that corrosion/precipitation depends on both the local and global

conditions. However the present models only consider mass transport process in flowing LBE and the interface dynamics (dissolution of steel or formation and dissociation of oxide) are assumed to be at local equilibrium. A general model should include both the mass transfer (of corrosion products and oxygen) in LBE and oxidation and scale removal at the steel/LBE interface, and incorporating surface modification effects by prolonged corrosion and deposition. Similar models for large and/or natural convection systems should be developed since they have markedly different flow characters from that of loop systems. Also, a numerical model should be developed to study localized flow effects on corrosion in regions where the flow changes direction sharply or where there are vortices.

In conclusion, a review of the fundamental issues in lead-alloys corrosion is provided with an emphasis on aspects deemed relevant in materials and technology development for applications. It is hoped that a succinct summary of important materials properties, experimental results, key techniques and current understanding through modeling will help advance the state of art in this field with important technological implications through rational design and selection.

8. References

- [1] HANSEN, M., ANDERKO, K., *Constitution of Binary Alloys*, McGraw-Hill Book Co., Inc., New York (1958).
- [2] ELLIOTT, R.P., *Constitution of Binary Alloys*, I-Supplement, McGraw-Hill Book Co., Inc., New York (1965).
- [3] HULTGREN, R., DESAI, P.D., HAWKINS, D.T., GLEISER, M., KELLEY, K.K., *Selected values of the thermodynamic properties of binary alloys*, American Society for Metals, Metals Park, Ohio (1973) 436-445.
- [4] ORLOV, Y.I., *Proceedings: International Workshop on Physics of Accelerator-Driven Systems for Nuclear Transmutation and Energy Production*, Trento, Italy, Sept. 29-Oct. 3, 1997.
- [5] GONSER, U.Z., *Phys. Chem. (Frankfurt)* **1** (1954) 1.
- [6] PRASAD, R., VENUGOPAL, V., SOOD, D.D., *J. Chem. Thermodynamics* **9** (1977) 765.
- [7] ORLOV, Y.I., *The main impurities and their condition in the Pb-Bi coolant*, contract SSC RF IPPE/CEA-DRN-DER 5010 6 8 B049630, Substage 2.1, Obninsk (1998).
- [8] OKAJAMA, K., SAKAO, H., *Trans. Jap. Inst. Metals* **9** (1968) 325.
- [9] ELLIOT, J.F., CHIPMAN, J., *J. Am. Chem. Soc.* **73** (1951) 2682.
- [10] MOSER, Z., *Z. Metallkde* **64** (1973) 40.
- [11] MIKULA, A., *Monatshefte Fur Chemie* **117** (1986) 1379.
- [12] FRUEHAN, R., *J. met. Trans.* **2** (1971) 1213.
- [13] MEHROTA, G.M., FROHBERG, M.G., KAPOOR, M.L., *Z. Metallkde* **67** (1976) 186.
- [14] LI, N., *Lead-Bismuth Eutectic (LBE) Materials Test Loop (MTL) Test Plan*, Los Alamos National Laboratory, LA-UR-01-4866 (2001).
- [15] U.S. DEPARTMENT OF ENERGY, *A Roadmap for Developing Accelerator Transmutation of Waste (ATW) Technology – A Report to Congress*, DOE/RW-0519, October 1999.
- [16] WEEKS, J.R., *Nuclear Engineering and Design* **15** (1971) 363.
- [17] ADAMOV, E.O., ORLOV, V.V., “Nuclear Power Development on the Basis of New Concepts of Nuclear Reactors and Fuel Cycle,” *Proceedings of Heavy Liquid Metal Coolants in Nuclear Technology* (HLMC-98), Vol. 1., Obninsk, SSC RF-IPPE (1999) 24.
- [18] HULTGREN, R., ORR, R.L., ANDERSON, P.D., KELLEY, K.K., *Selected Values of Thermodynamic Properties of Metals and Alloys*, Wiley, New York, 1963.
- [19] STRAUSS, S.W., RICHARDS, L.E., BROWN, B.F., *Nucl. Sci. Engin.* **7** (1960) 422.
- [20] GEBHARDT, E. et al., *Z. metallkde* **46** (1955) 90.
- [21] NUCKER, N., ANGEW, Z.F., *Physik.* **27**(1), (1969) 33.
- [22] OFTE, D., WITTENBERG, L.J., *Trans. Uet. Coc. AIME* **227** (1963) 706.
- [23] DAVIS, C.D., SHIEH, A.S., Presented at ICONE-8, April 2-6, 2000, ICONE-8220.

- [24] KAPLUN, B., SHULAEV, V.M., LINKOV, S.P., VARLLAMOV, Y.D., "The Viscosity of Lead-Bismuth Eutectic Alloy," *Teplofiz. Svoistva Veshestv Mater. Novosibirsk* **105** (1979).
- [25] CHHABRA, R.P., SHETH, D.K., *Z. metallkde* **81** (1990) 264.
- [26] Kutateladze, S.S., Borishanskii, V.M., Novikov, I.I., Fedynskii, O.S., *Liquid Metal Heat Transfer Media*, Consultants Bureau, Inc., New York (1959).
- [27] NIKOL'SKII, N.A. et al. "Thermal and Physical Properties of Molten Metals and Alloys," in *Problems of Heat Transfer* written by M. A. Mikheev, Academy of Sciences SSSR, Moscow (1959) 1-38.
- [28] TANIGAKI, M. et al., *Journal of Chemical Engineering of Japan* **16**(2), (1983) 92.
- [29] NIWA, K. et al., *Journal of Metals* **209** (1957) 86.
- [30] GRACE, R.E., DERGE, G., *Journal of Metals* **203** (1955) 839.
- [31] KOHL, J.G., *Zeitschrift fur Metallkunde* **71**(5), (1980) 325.
- [32] WEEKS, J.R., "Mechanisms of Liquid Metal Corrosion," 4th NASA-AEC Liquid Metal Corrosion Meeting, CONF-428, October 2, 1963.
- [33] TORTORELLI, P.F., CHOPRA, O.K., *Journal of Nuclear Materials* **103** (1981) 621.
- [34] LYUTYI, E.M., *Soviet Union Materials Science* **24** (1988) 441.
- [35] MAKSIMOVICH, G.G., LYUTYI, E.M., BOBYK, R.I., FIZ-KHIM, M., *Mater.* **2** (1983) 104.
- [36] REMY, F.N., BOUCHACOURT, M., *Nuclear Engineering* **133** (1992) 23.
- [37] HEITZ, E., *Corrosion* **47**(2), (1991) 135.
- [38] WEEKS, J.R., *ASM Trans. Quart.* **58** (1965) 302.
- [39] LI, N., *Active Control of Oxygen in Molten Lead-Bismuth Eutectic Systems to Prevent Steel Corrosion and Coolant Contamination*, Los Alamos National Laboratory, LA-UR-99-4696 (1999).
- [40] WEEKS, J., ROMANO, A.J., *Corrosion* **25**(3), (1969) 131.
- [41] EPSTEIN, L.F., *Liquid Metal Technology* **20** (1957) 67.
- [42] BANERJEE, S., *Proceedings: 5th International Congress on Metallic Corrosion*, Tokyo, Japan, May 21-27, 1974.
- [43] ROBERTSON, W.M., *Trans. TMS-AIME* **242** (1968) 2139.
- [44] BALBAUD-CELERIER, F., BARBIER, F., *Journal of Nuclear Materials* **289** (2001) 227.
- [45] EINSTEIN, A., *Annalen Der Physik* **17** (1905) 549.
- [46] GLASSTONE, S., LAIDIER, K., EYRING, H., *The Theory of Rate Processes*, McGraw-Hill Book Co. Inc., New York (1941) 447.
- [47] ROTHMAN, S.J., HALL, L.D., *Journal of Metals* **206** (1956) 199.
- [48] GUMINSKI, C., *Liquid Metal Systems*, H.U. BORGSTEDT, G. FREES (Eds.), Plenum, New York (1995) 345.
- [49] ILINCEV, G., *Nuclear Engineering and Design* **217** (2002) 167.
- [50] HE, X., LI, N., MINEEV, M., *Journal of Nuclear Science* **297** (2001) 214.
- [51] ZHANG, J., LI, N., *Nuclear Technology* **144** (2003) 379.
- [52] PARK, J.J. et al., *Nuclear Engineering and Design* **196** (2000) 315.
- [53] WEEKS, J.R., KLAMUT, C.J., *Nuclear Science and Engineering* **8** (1960) 133.
- [54] ROMANO, A., KLAMUT, C.J., GURINSKY, D.H., *The investigation of container materials for Bi and Pb alloys. Part I. Thermal convection loops*, BNL-811 (T-313), 1963.
- [55] LI, N., *Journal of Nuclear Materials* **300** (2002) 73.
- [56] GORYNIN, I.V., KARZOV, G.P., MARKOV, V.G., LAVRUKHIN, V.S., YAKOVLEV, V.A., "Structure Materials for Power Plants with Heavy Liquid Metals as Coolants," *Proceedings: Heavy Liquid Metal Coolants in Nuclear Technology*, Vol. 1 (HLMC-98), Obninsk, Russia, 120.
- [57] CHANG, Y.A., FITZNER, K., ZHANG, M., *Progress in Materials Science* **32** (1988) 97.
- [58] WAGNER, C., *Thermodynamics of Alloys*, Addison Wesley, Reading, Massachusetts (1952).
- [59] TASKINEN, A., *Z. metallk.* **73** (1982) 163.
- [60] OTSUKA, S., KUROSE, Y., KOZUKA, Z., *Metall. Trans.* **15B** (1984) 141.
- [61] ANIK, S., FROHBERG, M.G., *Phy. Chem.* **91** (1987) 790.

- [62] GROMOV, B.F., ORLOV, Y.I., MARTYNOV, P.N., GULEVSKY, V.A., "The Problems of Technology of the Heavy Liquid Metal Coolants (Lead-Bismuth, Lead)," *Proceeding: Heavy Liquid Metal Coolants in Nuclear Technology*, Vol. 1 (HLMC-98), Obninsk, Russia, 87.
- [63] SZWARC, R., OBERG, K.E., RAPP, R.A., *High Temperature Science* **4** (1972) 347.
- [64] ALCOCK, C.B., BEDFORD, T.V., *Trans. Farad. Soc.* **60** (1964) 822.
- [65] CHARLE, H., OSTERWALD, J., *Zeitschrift Fur Physikalische Chemie Neue Folge. Bd.* **99** (1976) 199.
- [66] FITZNER, K., *Thermochemica ACTA* **35** (1980) 277.
- [67] HAHN, S.K., STEVENSON, D.A., *J. Chem. Thermodynamics* **11** (1979) 627.
- [68] HESHMATPOUR, B., STEVENSON, D.A., *J. Electroanal. Chem.* **130** (1981) 47.
- [69] SAMSONOV, G.V., *The Oxide Handbook*, IFI/Plenum, New York-Washington-London (1973).
- [70] LEFHALL, C.H., KNEBEL, J.U., MACK, K.J., *Journal of Nuclear Materials* **296** (2001) 301.
- [71] HONMA, S., SANO, N., MATSUSHITA, Y., *Metallurgical Transactions* **2** (1971) 1494.
- [72] ARCELLA, F.G., FITTERER, G.R., *Journal of Metals* **20** (12), (1968) 47A.
- [73] RICAPITO, I., FAZIO, C., BENAMATI, G., *Journal of Nuclear Materials* **301** (2002) 60.
- [74] MULLER, G., SCHUMACHER, G., ZIMMERMANN, F., *Journal of Nuclear Materials* **278** (2002) 85.
- [75] MULLER, G., HEINZEL, A., SCHUMACHER, G., WEISENBURGER, A., *Journal of Nuclear Materials* **321** (2003) 256.
- [76] FERNANDEZ, J.A., ABELLA, J., BARCELO, J., VICTORI, L., *Journal of Nuclear Materials* **301** (2002) 47.
- [77] KONYS, J., MUSCHER, H., VOB, Z., WEDEMEYER, O., *Journal of Nuclear Materials* **296** (2001) 289.
- [78] GHETTA, V., FOULETIER, J., HENAULT, M., LE MOULEC, A., *J. Phys. IV France* **12**(8), (2002) 123.
- [79] COUROUAU, J.L., DELOFFRE, P., ADRIANO, R., *J. Phys. IV France* **12**(8), (2002) 141.
- [80] LI, N., HANG, W., DARLING, T., *Proceedings of the 11th International Conference on Nuclear Engineering* (ICONE11-35561), Tokyo, Japan, April 20-23, 2003. Accepted by *Journal of Nuclear Science and Technology*.
- [81] SHMATKO, B.A., RUSANOV, A.E., *Materials Science* **36** (2000) 689.
- [82] BARBIER, F., BENAMATI, G., FAZIO, C., RUSANOV, A., *Journal of Nuclear Materials* **295** (2001) 149.
- [83] GLASBRENNER, H., KONYS, J., MUELLER, G., RUSANOV, A., *Journal of Nuclear Materials* **296** (2001) 237.
- [84] BALBAUD-CELERIER, F., BELOFFRE, P., TERLAIN, A., RUSANOV, A., *J. Phys. IV. France* **12**, (2002) Pr8-177.
- [85] FAZIO, C., RICAPITO, I., SCADDOZZO, G., BENAMATI, G., *Journal of Nuclear Materials* **318** (2003) 325.
- [86] FAZIO, C., BENAMATI, G., MARTINI, C., PALOMBARINI, G., *Journal of Nuclear Materials* **296** (2001) 243.
- [87] BENAMATI, G., FAZIO, C., PIANKOVA, H., RUSANOV, A., *Journal of Nuclear Materials* **301** (2002) 23.
- [88] MULLER, G. et al, *Journal of Nuclear Materials* **301** (2002) 40.
- [89] CRESPO, L.S., MARTIN MUNOZ, F.J., GOMEZ BRICENO, D., *Journal of Nuclear Materials* **296** (2001) 273.
- [90] BRICENO, D.G. et al., *Journal of Nuclear Materials* **296** (2001) 265.
- [91] BRICENO, D.G. et al., *Journal of Nuclear Materials* **303** (2002) 137.
- [92] ZHANG, J., LI, N., RUSANOV, A., *Journal of Nuclear Materials* (2004), in preparation.
- [93] LI, N., HE, X., RUSANOV, A., DEMISHONKOV, A.P., *Corrosion Test of U.S. Steels in Lead-Bismuth Eutectic (LBE) and Kinetic Modeling of Corrosion in LBE Systems*, Los Alamos National Laboratory, LA-UR-02-2028 (2002).
- [94] BARBIER, F., RUSANOV, A., *Journal of Nuclear Materials* **296** (2001) 231.
- [95] KTKINSON, A., *Reviews of Modern Physics* **57**(2), (1985) 437.
- [96] CORY, N.J., HERRINGTON, T.M., *Oxidation of Metal* **28**(5/6), (1987) 237.
- [97] PETERSEN, N.L., CHEN, W.K., WOLF, D.J., *J. Phys. Chem. Solids* **41** (1980) 709.
- [98] ZHANG, J., LI, N., *Journal of Nuclear Materials* **312** (2003) 184.

- [99] ZHANG, J., LI, N., *Journal of Nuclear Materials* **326** (2004) 201.
- [100] ZHANG, J., LI, N., *Corrosion* **60** (2004).
- [101] ZHANG, J., LI, N., *Journal of Nuclear Science and Technology* **41** (2004).
- [102] BERGER, F.P., HAU, K.F.F.L., *Int. J. Heat Mass Transfer* **20** (1977) 1185.
- [103] SILVERMAN, D.C., *Corrosion* **40** (1984) 220.
- [104] HARRIOTT, P., HAMILTON, R.M., *Chem. Eng. Sci.* **20** (1965) 1073.
- [105] SANNIER, J., SANTARINI, G., *Journal of Nuclear Materials* **107** (1982) 196.
- [106] KIKUCHI, K., KURATA, Y. et al., *Journal of Nuclear Materials* **318** (2003) 348.
- [107] BARTLETT, J.W., *Theory of Corrosion Product Generation, Dispersion and Activation Process*, U.S. Atomic Energy Commission Report BNWL 676, June 10, 1968.
- [108] CHARLESWORTH, D.H., *AIChE Chem. Eng. Prog. Symp. Ser.* **66**(104), (1970) 21.
- [109] SOMERSCALES, E.F.C., *Experimental Thermal and Fluid Science* **14** (1997) 335.
- [110] LYCZKOWSKI, R.W., BOUILLARD, J.X., *Progress in Energy and Combustion Science* **28** (2002) 543.